Università Politecnica delle Marche
Corso di laurea in Ingegneria Civile-Ambientale

ASSESSING THE HEALTH RISK DERIVING FROM EXPOSURE TO AIRBORNE POLLUTANTS

VALUTAZIONE DEL RISCHIO INCREMENTALE DERIVANTE DALL'ESPOSIZIONE A INQUINANTI AERIFORMI

Coordinator:

Prof. Eng. Giorgio Passerini

Advisor:

Dr. Enrico Mancinelli

Student: MAHASSEN RAMADAN

Academic year 2019/2020

Contents

1- Introduction

Air is a mixture formed by gas, mainly nitrogen and oxygen, and particles of various nature and dimensions, which constitute the earth's atmosphere.

Nitrogen (N_2) represents about 78% of the total molecules of the Earth's atmosphere and oxygen (O_2) about 21%. The remaining part of the atmosphere consists of 0.93% argon (Ar), 0.03% carbon dioxide (CO_2) and other gases in much lower percentages.

99% of the earth's atmosphere mass is included in the first 30 km. This air mass protects us from ultraviolet radiation, from the impact of high-energy particles from space and from temperature changes that could make the environmental conditions of the surface prohibitive.

Most of the pollutants emitted, which can have harmful effects on human health or the environment as a whole, are detected in the lower part of the atmosphere, called the troposphere.

Air pollution is an environmental issue of public health concern. Exposure to air pollutants in urban areas, emitted by different sources, can cause severe health problems such as increased morbidity and mortality and alterations in the respiratory, cardiovascular and cerebrovascular systems.

1.1 Sources and emissions of air pollutants

Fig 1: Spatial distribution of NO_2 in different weather conditions evidence pollutants different origin and diffusion. (Ielpo et al. 2019)

Air pollutants may be categorised as primary or secondary.

Primary pollutants are directly emitted to the atmosphere, whereas secondary pollutants are formed in the atmosphere from precursor pollutants through reactions. Air pollutants may have a natural, anthropogenic or mixed origin, depending on their sources or the sources of their precursors.

Key primary air pollutants include PM, NO_x (which includes both NO and NO_2), methane (CH_4), non-methane volatile organic compounds (NMVOCs) including C_6H_6, certain metals and polycyclic aromatic hydrocarbons (PAH, including BaP).

Key secondary air pollutants are PM (formed in the atmosphere), NO_2 and a number of oxidised VOCs. Key precursor gases for secondary PM are SO_2, NO_x, NH_3 and VOCs. The gases NH_3, SO_2 and NO_x react in the atmosphere to form NH_4^+, SO_4^{2-} and NO_3^- compounds. These compounds form new particles in the air or condense onto pre-existing ones to form secondary PM (also called secondary inorganic aerosols). Certain NMVOCs are oxidised to form less volatile compounds, which form secondary organic aerosols. Ground-level (tropospheric) O_3 is not directly emitted into the atmosphere. Instead, it is formed from chemical reactions in the presence of sunlight, following emissions of precursor gases, mainly NOx, NMVOCs and CH_4. These precursors can be of both natural (biogenic) and

anthropogenic origin. NO_x also depletes tropospheric O_3 as a result of the titration reaction with the emitted NO to form NO_2 and oxygen

1.2 Airborne pollutants (NO_x , PM)

The growing industrial development, the increase in emissions of combustion products, the increasingly large urban agglomerations are only some of the causes of one of the most serious problems of modern society: air pollution.

The EEA (European Environment Agency) defines pollution as the alteration, directly or indirectly caused by man, of the biological, physical, chemical properties of the environment, when a risk or potential risk to the health of the environment is created man or the safety and well-being of every living species. Air pollution is the alteration of the natural air conditions due to the emission of polluting compounds into the atmosphere.

The sources of pollution can be natural (volcanic eruptions that release SO_2, fires in which PM_{10} is released) or anthropogenic (activities of human origin).

The principals airborne pollutants are:

1.2.1- Nitrogen oxides (NO_x), Potential Source both Natural And Anthropogenic

generated in the combustion processes of motor vehicles, in power plants and in heating systems. They cause respiratory diseases, photochemical smog and acid rain. The main compounds that contain nitrogen are:N_2O, NO, NO_2, NH_3, HNO_3, $HONO$, $N_2O_5$and the salts of NO_3, NO_2, NH_4. The most abundant of these in the atmosphere is NO_2

Fig 2: The Electronic Dot Structure for mono-nitrogen di- oxygen. (Lian et al. 1998)

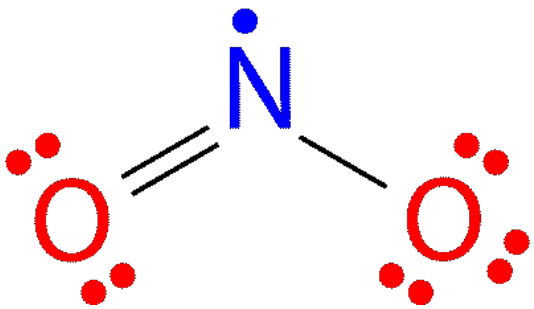

Nitrogen dioxide (NO_2): is one of a group gases called nitrogen oxides (NO_x). While all of these gases are harmful to human health and the environment, where NO_2 is greater concern. Other nitrogen oxides include nitrous acid and nitric acid. NO_2 is used as the indicator for the lager group of nitrogen oxides. It is consider into chemical compound with formula NO_2. It is one of these gases created their main causes is from the burning of fossil fuels like gas and coal. Nitrogen dioxides occurs when nitrogen molecules or N_2 and oxygen molecules or O_2 to combine in situations that happen in an extremely hot environment this means that everything that uses gas like electricity in the cars produce nitrogen dioxide.

Nitrogen dioxide (NO_2) plays a fundamental role in the formation of photochemical smog as it is the intermediary for the production of dangerous secondary pollutants such as ozone, nitric acid and nitrous acid.

These, once formed, can be deposited on the ground wet (for example acid rain) or dry causing damage to vegetation and buildings.

Nitrogen oxides, in particular dioxide, are also gases harmful to human health as they can cause acute health effects, in particular:

- acute such as respiratory dysfunction and bronchial reactivity (mucosal irritations);

- chronic such as changes in lung function and increased risk of cancer.

The subjects most at risk are children and people already suffering from diseases of the respiratory system (asthmatics), as well as those living near roads with high traffic density due to long-term exposure.

On a global scale, emission of nitrogen oxides from natural sources far outweigh those generated by human activities. Natural sources include intrusion of stratospheric nitrogen oxides, bacterial and volcanic action, and lightning. Because natural emission are distributed over the entire surface of the earth, however, the resulting background atmospheric concentration are very small. The major source of anthropogenic emissions of nitrogen oxides into the atmosphere is the combustion of fossil fuels in stationary sources (heating, power generation) and in motor vehicles (internal combustion engines).

Other contributions of nitrogen dioxide to the atmosphere comes from specific non-combustion industrial processes, such as the manufacture of nitric acid, the use of explosives and welding.

Indoor sources include tobacco smoking and the use of gas fired appliances and oil stoves.

Fig 3: Anthropogenic sources of NO_2 (Volkamer et al. 2006)

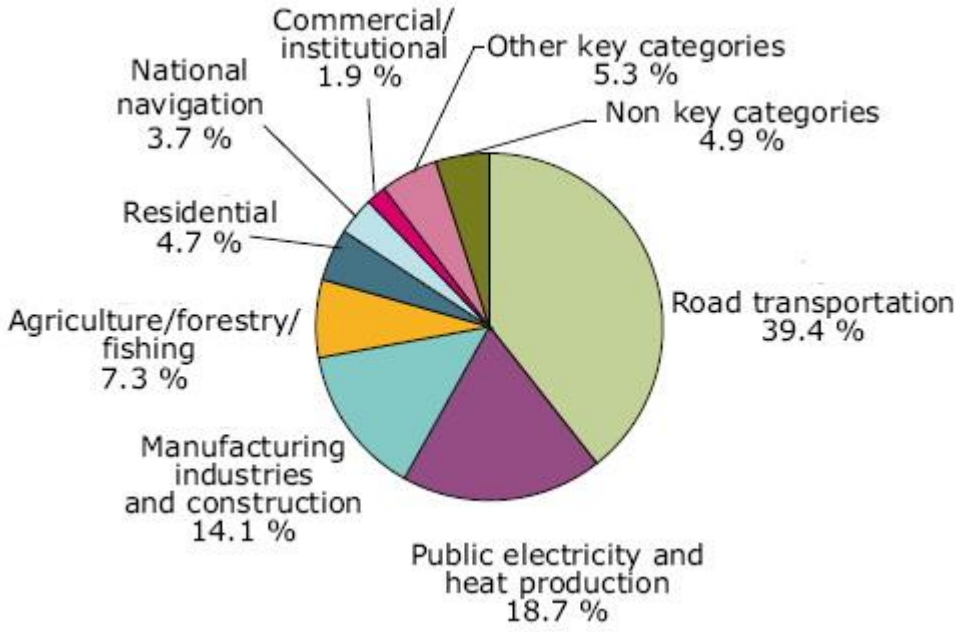

1.2.2 Particulate Matter (PM)

Fine dust: they can be compared to a slow and silent killer, they are so small that they can be inhaled and gradually accumulate in the respiratory system. When we talk about fine dust we usually refer to the so-called PM_{10}, but in the last ten years scientists have highlighted another form of pollution related to fine dust with a smaller diameter, $PM_{2.5}$ the abbreviation particulate matter (PM) identifies material that is present in the atmosphere in the form of microscopic particles. PM, whose aerodynamic diameter is equal to or less than 10 µm, is termed PM_{10}.

It consists of dust, smoke, micro-drops of liquid substances called in aerosol technical jargon: in fact, it is a set of particulates, or solid and liquid particles dispersed in the air with relatively small dimensions. These particles present in the atmosphere are indicated by many common names: dust and soot for solid ones, mist and fog for liquid ones.

$PM_{2.5}$- fine particulate with a diameter less than 2.5 μm (a quarter of a hundredth of a millimeter), is a thoracic powder, that is able to penetrate deeply into the lungs, especially during breathing from the mouth.

Therefore $PM_{2.5}$ is a subset of PM_{10}, which in turn is a subset of the coarse particulate, etc.

Airborne particle matter (PM) is one of the air pollutants of primary health concern. Over the past two decades, PM mass metrics (e.g., particles with aerodynamic diameter 10 μm, PM_{10}, and particles with aerodynamic diameter 2.5 μm, $PM_{2.5}$) have received much attention, and many studies have shown that high concentrations of PM are associated with increased risks of mortality and morbidity. More recently, the evidence derived from studies of long- and short-term exposure has been judged sufficient to infer causality for fine particles (EPA, 2012; WHO/Europe, 2013 cited by Pirani et al. 2015).

1.3- Air pollution exposure with children's health

In an increasingly urbanized world, more children are living in cities. Indeed, demographic trends indicate that the world's urban population will double by 2050. In spite of a number of socioeconomic benefits, urbanization has been associated with adverse health effects mainly due to increasing exposure to air pollution. Children are particularly vulnerable to the impacts of environmental exposures because childhood is a period of rapid growth and development and because children breathe more per body kilogram and are more physically active than adults.
Environmental factors play an important role in the worldwide increasing prevalence of respiratory and allergic diseases observed during the last decades. In particular, asthma and rhino-conjunctivitis largely contribute to the global burden of disease, with a global prevalence in schoolchildren ranging from < 5 to > 20% and from 0.8 to 39.7%, respectively. (cited by Cilluffo et al. 2018)

Because of increasing urbanization, there is growing interest in factors affecting environmental exposures within urban settings, such as traffic intensity, household density and natural and green space. All these factors were taken into account. The role of both residential surrounding greenery and proximity to green spaces (i.e. 'greenery') on respiratory and allergic symptoms in schoolchildren has so far yielded inconsistent results, likely due to differences in exposure timing or in greenery type among different studies.

The built environment in urban areas (i.e. 'grey' surfaces, which comprise industrial, transport and urban features) appears to have side effects on children's health, mainly due to increasing exposure to air pollution, noise and high temperatures, lower access to natural environments, and accentuated sedentary life. Apart from air pollution, there have been few investigations on the association between "urbanicity" and respiratory and allergic symptoms in childhood.

Land Use Regression (LUR) models have been used for estimating outdoor air pollution concentrations at the home addresses in order to analyze their association with respiratory health. Significant associations between NO_2, LUR and non-atopy related asthma and wheezing were found in aged 6–7 years girls and 13–14 years female adolescents from randomly selected schools in Hamilton, Canada. Notably, the association between NO_2 exposure and health outcomes has been shown not to depend on the type of model used to estimate exposure.

2-DISCUSSIONS

2.1- The effect of NO_2 emissions on different urban sites

Fig 4: Slight decrease or no change in NO_2 concentrations at the studied sites. (Casquero-Vera et al. 2019)

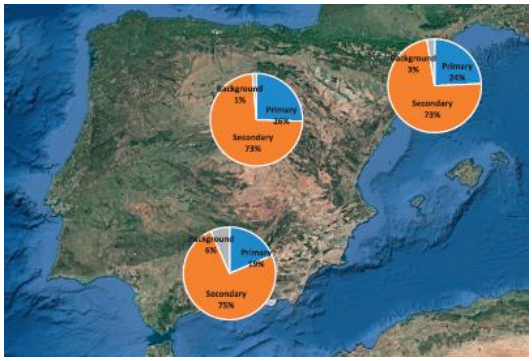

A large part of the population lives in urban areas, therefore, the failure of EU emission control measures to reduce NO_2 ambient concentrations in urban areas has important implications for public health. NO_2 is a toxic gas, mainly formed in the atmosphere by reactions of NO and ozone, although direct NO_2 emissions by traffic, especially diesel fueled vehicles, can also contribute to ambient NO_2 concentration.

High ambient NO_2 concentrations can cause inflammation of the airways and cardiovascular, and even morbidity and mortality.
According to the last European Environment Agency report, NO_2 was responsible for 71,000 premature deaths in EU and for 4,280 premature deaths in Spain in 2013. Also, NO_2 contributes to the formation of secondary aerosols and tropospheric ozone in the atmosphere, which also have adverse impacts on human health.
Several studies have shown that NO_2 yearly and hourly exceedances are caused by road traffic emissions (e.g., Degraeuwe et al., 2016; Querol et al., 2014; Wild et al., 2017 cited by Casquero-Vera et al. 2019). Some studies in the UK, Switzerland, Finland and Germany have attributed the weaker downward trends of NO_2 and the non-compliance of NO_2 air quality standards in urban areas to the significant increase of the number of diesel-fueled vehicles together with the increase of primary NO_2 fraction in the NO_x exhaust from diesel vehicles fitted with modern after exhaust treatment technologies.

The NO_2 fraction in the total NO_x emitted (f- NO_2) by diesel vehicles not fitted with modern exhaust treatment technologies is about 10-12% and can reach up to 70% for those fitted with particle traps and oxidation catalysts like EURO III, IV, V, VI (Carslaw et al., 2016 cited by Casquero-Vera et al. 2019). Using an urban NO_2 pollution model with various NO_x emission scenarios, found that the reduction in NO_x emissions of diesel cars is more relevant than the NO_2 fraction in the total NO_x emissions for the reduction of regional and urban NO_2 concentrations. However, Henschel et al. (2015 cited by Casquero-Vera et al. 2019) could not draw any clear conclusion concerning the role of primary NO_2 emissions or other factors in the observed NO_2 trends at 9 European cities, recommending further research to explore the potential factors affecting the observed trends in ambient NO_2 concentrations in urban areas.

2.1.1- The impact of air pollution on human health long- and short-term

The impact of air pollution on human health is well documented through long- and short-term epidemiological cohort studies. Air pollution from NO_2 in the cities has important effects on public health, summarized in two types of conditions. On the one hand, air pollution results in increased morbidity, especially by cardiovascular and respiratory diseases. McConnell et al. (2003 cited by Casquero-Vera et al. 2019) studied the long-term exposure to NO_2 and the appearance of bronchitis symptoms in asthmatic children, while Anderson et al. (2007 cited by Casquero-Vera et al. 2019) studied the associated short-term exposure to NO_2 and hospital admissions for respiratory diseases.

However, despite the identified relationship between health effects and air pollution, recent epidemiological studies emphasized the difficulties in interpreting any health-related dataset when information on the intra-urban variability of pollution is not available.

Table 1: Resume of principal information about the work by Casquero-Vera et al. 2019

Sites	Method	Aim	Period	Limit
Barcelona, Madrid, Granada	quantify the contributions of primary NO_2 emissions, photo-chemically formed NO_2 and background concentrations	estimate of the concentration of NO_x that needs to be reduced to comply NO_2 limits.	2003 - 2014	40 µg/m³

Table 1 shows the Resume of principal information used for the study of NO_x concentration in the three cities of Spain and the effect of NO_2 emissions on different urban sites. In order to determine f-NO_2 (fraction of NO_2 in the total NO_x emissions) at the studied traffic sites from ambient monitoring data was use the model developed by Abbott (2005 cited by Casquero-Vera et al. 2019). This method has the advantage that it is based on a mathematical representation of the physical and chemical processes involving NO, NO_2 and O_3 in the atmosphere. It requires ambient measurements of NO, NO_2 and O_3 concentrations at traffic and at nearby background site. This method removes the effect of background pollution by considering the difference in the O_x ($O_3 + NO_2$) and NO_x (NO + NO_2) concentrations between an urban traffic station and a nearby background station. A more detailed description of the model is provided in Supplementary Material; although, a brief description is given below.

In Abbott (2005 cited by Casquero-Vera et al. 2019) model, f-NO_2 is obtained from the following regression
equation:

$$[\boldsymbol{O_x}]_{\boldsymbol{Local}} = \boldsymbol{a}[\boldsymbol{NO_x}]_{\boldsymbol{Local}} + \boldsymbol{b} \quad \textbf{(1)}$$

Where $[\boldsymbol{O_x}]_{\boldsymbol{Local}}$ and $[\boldsymbol{NO_x}]_{\boldsymbol{Local}}$ are defined as follow:

$$[\boldsymbol{O_x}]_{\boldsymbol{Local}} = [\boldsymbol{NO_2}]_{\boldsymbol{TR}} + [\boldsymbol{O_3}]_{\boldsymbol{Local}} - [\boldsymbol{NO_2}]_{\boldsymbol{RB}} - [\boldsymbol{O_3}]_{\boldsymbol{RB}} \quad \textbf{(1.1)}$$

$$[\boldsymbol{NO_x}]_{\boldsymbol{Local}} = [\boldsymbol{N0}]_{\boldsymbol{TR}} + [\boldsymbol{No_2}]_{\boldsymbol{TR}} - [\boldsymbol{NO}]_{\boldsymbol{RB}} - [\boldsymbol{NO_2}]_{\boldsymbol{RB}} \quad \textbf{(1.2)}$$

where $[\mathrm{NO}]_{\mathrm{TR}}$, $[NO_2]_{TR}$ and $[O_3]_{TR}$ are the concentrations of NO, NO_2 and O_3 (in ppb) at the traffic station and $[\mathrm{NO}]_{\mathrm{RB}}$, $[NO_2]_{RB}$ and $[O_3]_{RB}$ are the corresponding concentrations in the nearby background station.

The regression parameter **a** provides the fraction of NO_2 in the total NO_x emissions (f- NO_2), and **b** is the intercept parameter which is expected to be close to zero. The parameter **b** excludes the background oxidant concentrations and represents the net effect of deposition and other chemical and photochemical reactions (different of O_3 +NO − > NO_2 and photodissociation of NO_2) that contribute to a lesser extent to ambient NO_x and O_3 concentrations. It is worth noting that both parameters **a** and **b** are relatively insensitive to the choice of background monitoring site as was showed by Abbott (2005 cited by Casquero-Vera et al. 2019).
In this study, linear regression analysis on each annual set of hourly [Ox]local and [NOx]local data was done to retrieve f- NO_2 for each year at BCN(TR), GRA(TR) and MAD(TR) sites using BCN(RB), GRA(RB) and MAD(RB) as nearby background sites. The results show that for all_analysed sites, despite the scatter, there is a good correlation between $[O_x]$local and $[NO_x]$local in each dataset. Also, the values of intercept parameter **b** are, as expected, very small and close to zero, suggesting_that BCN(RB), GRA(RB) and MAD(RB) sites are representative of background_conditions for BCN(TR), GRA(TR) and MAD(TR)sites, respectively.
After the estimation of f- NO_2 we determined the primary and secondary NO_2 concentrations at each traffic station (Anttila et al., 2011 cited by Casquero-Vera et al. 2019). In this calculation we assumed that the total NO_2 concentration observed

at each station is composed of primary NO_2 emission ($[NO_2]_{primary}$), secondary NO_2 formed by NO-O_3 reaction ($[NO_2]_{secondary}$) and regional background ($[NO_2]_{RB}$):

$$[\boldsymbol{NO_2}] = [\boldsymbol{No_2}]_{\boldsymbol{Primary}} + [\boldsymbol{NO_2}]_{\boldsymbol{secondary}} + [\boldsymbol{NO_2}]_{\boldsymbol{RB}} \quad \textbf{(2)}$$

Where

$$[\boldsymbol{NO_2}]_{\boldsymbol{Primary}} = \boldsymbol{a} \cdot [\boldsymbol{NO_x}]_{\boldsymbol{Local}} \quad \textbf{(2.1)}$$

$$[\boldsymbol{NO_2}]_{\boldsymbol{secondary}} = (\boldsymbol{1} - \boldsymbol{a}) \cdot [\boldsymbol{NO_x}]_{\boldsymbol{Local}} + [\boldsymbol{N0}]_{\boldsymbol{RB}} - [\boldsymbol{NO}]_{\boldsymbol{TR}} \quad \textbf{(2.2)}$$

Finally, to estimate the required NO_x reduction to achieve the NO_2 European standard limits at BCN(TR), MAD(TR) and GRA(TR) stations we used the roll-back model (De Nevers and Morris, 1975; Lu, 2004; Chaloulakou et al., 2008 cited by Casquero-Vera et al. 2019):

$$\mathrm{R}(\%) = \frac{(\mathrm{CA}-\mathrm{CR})}{(\mathrm{CA}-\mathrm{B})} \quad \textbf{(3)}$$

where **R (%)** is the necessary NO_x emission reduction, **CA** is the actual NO_x mean annual concentration (2014 in this work) and **CR** is the NOx mean concentration corresponding to the necessary reduction level (NO_x objective level). Finally, **B** is the NOx background concentration at traffic station. The background concentration in this equation corresponds to the concentration at traffic site when nearby source emissions that influence the NO_x concentration at this site are switched off. The values of **B** in this case were estimated from the concentrations observed at the three studied traffic stations. For this we calculated the mean hourly annual diurnal NO_xconcentrations at each studied traffic station for 2014. The minimum NO_x hourly concentration observed at each studied traffic station was taken as NO_x

background concentration at this site. The NO_x background concentrations of 47,39 and 30 µg/m³ were obtained for BCN(TR), MAD(TR) and GRA(TR), respectively**.** The roll-back model is widely used due to its simplicity and because it requires very little input data. This model assumes that the spatial distribution of emission sources, meteorological conditions and species are conservative. The NO_x can be considered stable for roll-back modelling, since the transformations are mainly internal to the cycle NO/ NO_2/O_3. The value of **R (%)** calculated by this model becomes indeterminate when the actual NOx annual mean concentration **(CA)** is similar to the NO_x background concentration **(B)**. Therefore, this method is limited to those situations where **CA** is higher than **B**. In addition, **CR** should be higher than **B** due to the impossibility to reduce NO_x concentration below the background concentration.

2.1.2- Results

Table 2: Details of the traffic and regional background stations with availability of NO, NO_2 and O3 data in the period 2003–2014.(Casquero-Vera et al. 2019)

Area	Station			Location		
	Name	Code	Type	Lat.	Long.	Height (m a.s.l)
Barcelona	Barcelona (Gracia-S. Gervasi)	ES1480A	TR	41.399	2.153	57
	Cabo De Creus	ES0010R	RB	42.319	3.316	23
Granada	Granada Norte	ES1560A	TR	37.196	−3.613	689
	Viznar	ES0007R	RB	37.237	−3.534	1230
Madrid	Escuelas Aguirre	ES0118A	TR	40.422	−3.682	672
	Campisábalos	ES0009R	RB	37.237	−3.534	1360

Table 3: Results of the Theil-Sen trend analysis for the 2003–2014 period. The symbols shown for the p values for each trend estimate relate to how statistically significant the trend estimate is: $p < 0.001$ = *** (highest statistical significance), $p < 0.01$= **, $p < 0.05$ = * and $p < 0.1$ = +; no symbol stands for no significant trend ($p > 0.1$). Units are μg $m^{-3}yr^{-1}$ for NO, NO2 and NOx, and yr^{-1} for NO/O3. (by Casquero-Vera et al. 2019)

	BCN_{TR}	GRA_{TR}	MAD_{TR}	BCN_{RB}	GRA_{RB}	MAD_{RB}
NO	-2.15^{***}	-0.52^{+}	-3.39^{***}	-0.01^{***}	-0.02^{***}	-0.01^{***}
NO_2	-1.85^{***}	0.02	-2.94^{***}	-0.03^{*}	-0.05^{*}	-0.04^{***}
NO_x	-4.16^{***}	−0.65	-6.74^{***}	-0.04^{***}	-0.08^{*}	-0.05^{***}
NO/O_3	-0.71^{***}	-0.03^{+}	-0.26^{***}	–	–	–

2.1.2.1- Levels of atmospheric pollutants

Fig. 5 shows the annual NO, NO_2 and NO_x concentrations and the NO/O_3 annual mixing ratio at TR stations and Table 3 summarizes trend analysis results at TR and RB station.

As expected, NO and NO_x concentrations at MAD(TR) and BCN(TR) stations were higher than those registered at GRA(TR) station during the whole studied period, due to their larger population and vehicles fleet. However, these differences in NO and NO_x concentrations between Madrid/Barcelona and Granada traffic stations decreased significantly along the study period (Fig. 5). These results show that there was significant reduction in NO and NO_x concentrations at Madrid and Barcelona traffic stations along the studied period in comparison to GRA(TR) station. Local/regional emission control measures to improve air quality started early in Madrid and Barcelona (e.g., ELCACM, 2006; PCACM, 2012, 2012; ECACCCM, 2014; and references therein cited by Casquero-Vera et al. 2019), however, in Granada these measures started in 2014.

High and statistically significant downward trends were observed for NO and NOx concentrations in Madrid and Barcelona cities, especially at traffic stations (Table 3), probably due to the implemented control measures, both local/regional control measures and EU directives. The NO and NO_x concentrations decreased by approximately 45% and 55%, respectively, between 2003 and 2014 in both MAD(TR) and BCN(TR) stations. In contrast, the reduction of NO and NO_x concentrations in GRATR was smaller and not statistically significant (Table 3).

As a result of the economic recession, the consumption of fuel oil used in diesel vehicles in Madrid, Barcelona and Granada in 2008–2014 decreased by 19%, 23% and 23%, respectively, with respect to 2003–2007 period. This high decrease in the consumption of fuel oil used by diesel vehicles, which are the main important source of NO_x in urban areas, was associated with a significant decrease in NO and NO_x concentrations in MAD(TR) and BCN(TR) stations during the economic recession. The NO concentrations in MAD(TR) and BCN(TR) decreased by 45% and 30%, respectively, while the NO_x decreased by 35% and 20%, respectively, in 2008–2014 compared to 2003–2007. However, although the percentage of reduction of the fuel oil consumption in Granada in 2008–2014 was similar to the recorded in BCN(TR) and MAD(TR), reductions of NO and NO_x concentrations in GRA(TR) were much smaller (22% and 10%, respectively) than those observed at MAD(TR) and BCN(TR). Granada is medium size and non industrialised city and, thus, the high reduction of the NO and NO_x in MAD(TR) and BCN(TR) stations during economic recession in comparison to GRA(TR) could be attributed to the reduction of NO_x emissions from industrial activities in Madrid and Barcelona cities.

Fig 5: 2003–2014 trends of mean annual (a) NO, (b) NO_2 and (c) NO_x concentrations (μg m^{-3}) and annual (d) NO/O3 mixing ratio recorded at BCNTR, GRATR and MADTR. (Casquero-Vera et al. 2019**)**

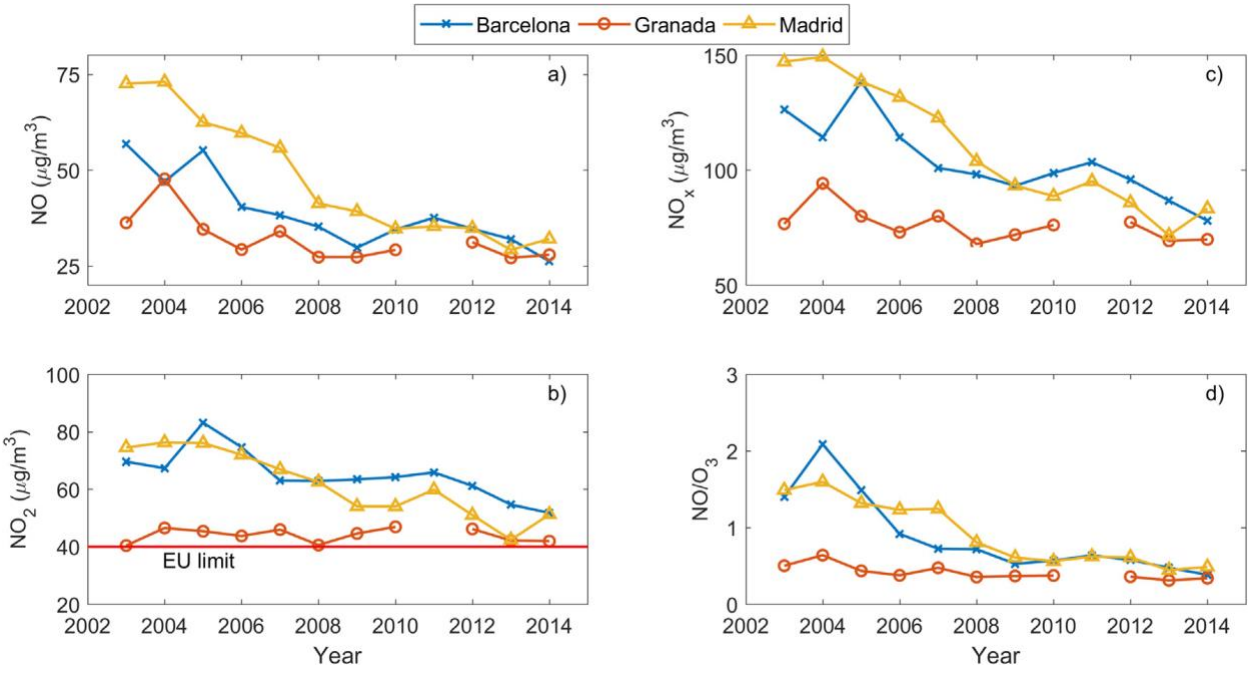

NO_2 concentrations over MAD(TR) and BCN(TR) stations showed clear statistically significant downward trends along the analysed period, decreasing by 30% and 25% over MAD(TR) and BCN(TR), respectively, from 2003 to 2014. However, the decrease in NO_2 concentrations observed over MAD(TR) and BCN(TR) stations was much less pronounced than the decrease in NO_x (55%) concentrations over both stations. By contrast, the annual NO_2 concentrations at GRA(TR) station were almost constant during the studied period (ranging from 40 to 47 μg m^{-3}) and don't show any statistically significant trend. It is worth to note that the annual NO_2 concentrations observed over MAD(TR) and BCN(TR) as well as over GRA(TR) stations is still exceeding the annual NO_2 standard limit of 40 μg m^{-3} established by EU for the human health protection in force since 2010 (Fig. 5). Therefore, the regulatory efforts done were insufficient and thus more stringent emission controls and efficient measures are still needed to improve air quality and to meet the European limit. The possible cause of the unexpectedly stabilization of NO_2 concentrations at GRA(TR) and of the weaker decreases of NO_2 concentrations at MAD(TR) and BCN(TR) stations and non-compliance of NO_2 air quality standards at these stations are investigated in the following sections.

2.1.2.2- Contributions of primary and secondary NO_2 to ambient

One of the possible reasons of the stabilization of NO_2 concentrations and the weaker decrease of NO_2 concentrations could be attributed to the increase of primary NO_2 fraction in the NO_x exhaust emissions from diesel vehicles fitted with modern after-exhaust treatment technologies. Primary NO_2 fraction in the total NO_x emissions (f-NO_2) at the studied traffic stations was estimated from Ambient monitoring data using the total oxidant method and the results are shown in Fig. 6. Primary NO_2 fraction values ranged from 8%, 11% and 3% in 2003 to 14%, 20% and 12% in 2006/2007 at MAD(TR), BCN(TR) and GRA(TR), respectively. Primary NO_2 fraction values obtained in this study are comparable to those found in other European cities. For example, Grice et al. (2009 cited by Casquero-Vera et al. 2019) estimated f-NO_2 values in the range 1.5–24% for various European sites in the period 2000–2005. Anttila et al. (2011 cited by Casquero-Vera et al. 2019) reported f-NO_2 values ranging from 7% to 20% in Helsinki for the period 1994–2008.

The largest f-NO_2 values were obtained at BCN(TR) station probably due to the influence of ship emissions from the Barcelona port. At GRA(TR) and MAD(TR) stations very similar f-NO_2 values were observed. As can be seen in Fig. 6, the f-NO_2 clearly increased from 2003 to 2006/2007 in all the studied traffic stations and slightly decreased or remained almost stable from 2007/2008 onwards. The main conclusion drawn from these results is that the increase of the f-NO_2 observed over the studied stations is, at least partly, one of the causes of the observed stabilization and the weaker decrease of NO_2 concentrations during the analised period. Another possible reason, supported by the decrease of the NO/O_3 (Fig. 5), could be the smaller reduction of the concentrations of secondary NO_2 compared to the NO, probably due to the change in the photo stationary state (e.g., Henschel et al., 2015 cited by Casquero-Vera et al. 2019).

Fig 6: The evolution of the annual f-NO_2 (%) in BCNTR, GRATR and MADTR stations during 2003–2014. The mean annual f-NO_2 (%) over the three studied sites is also included in the figure. (Casquero-Vera et al. 2019)

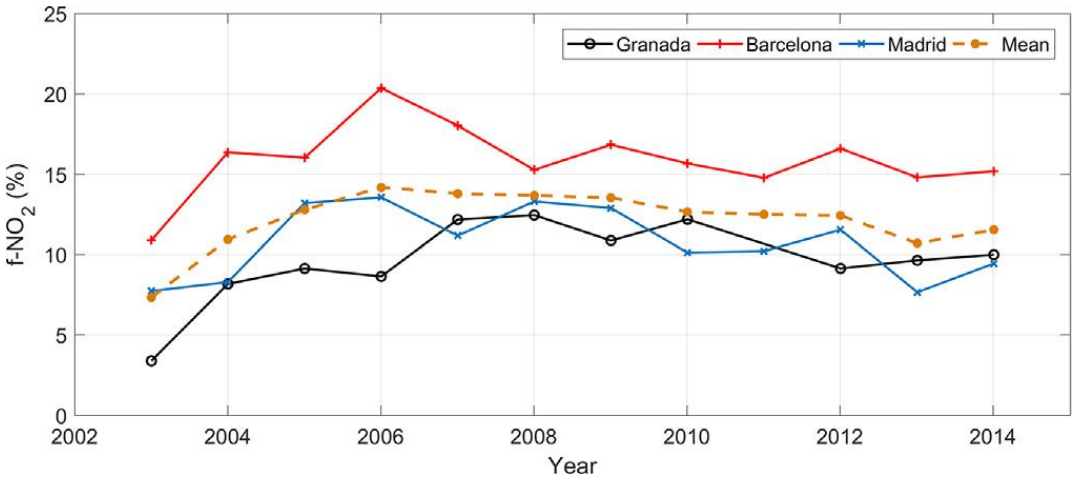

The estimated primary, secondary and background NO_2 concentrations at each station are shown in (Fig 7) As can be seen, the primary and secondary NO_2 concentrations at GRA(TR) remained fairly constant during the analysed period, with mean primary and secondary NO_2 concentrations (±standard diviation) of 8 ± 2 and 33 ± 2 μg m^{-3}, respectively. This result evidences that neither the primary nor the secondary NO_2 concentrations have decreased over the analysed period and points out that, in addition to the European control measures, the implementation of local/regional measures is necessary to improve air quality with respect to NO_2 in

this city. Since the annual ambient NO_2 concentrations at GRA(TR) (around 42 μg m^{-3} in 2013 and 2014) are very close to the NO_2 European standard limit, it would be expected that with additional local/regional abatement measures the annual standard limit would be achieved in the near future.

Fig 7: The estimated primary, secondary and background NO_2 concentrations at Barcelona, Granada and Madrid. Note that values are not integrated. (cited by Casquero-Vera et al. 2019)

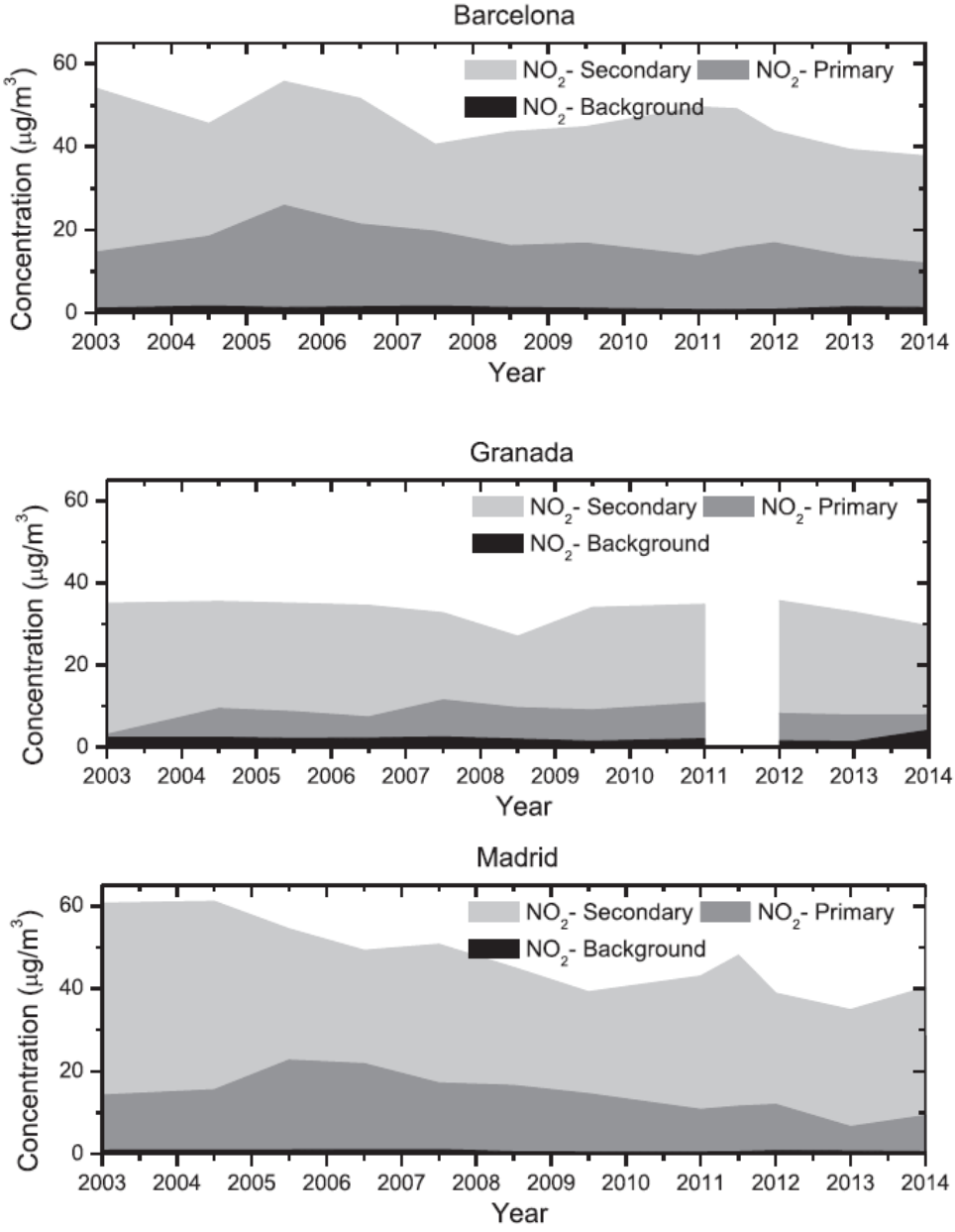

Primary NO_2 concentrations at BCN(TR) and MAD(TR) stations increased slightly from about 14 μg m^{-3} in 2003 to 22–26 μg m^{-3} in 2005 and then decreased slightly to about 12 μg m^{-3} in the last years (Fig 7). In contrast, secondary NO_2 concentrations at BCN(TR) and MAD(TR) decreased significantly over the period 2003–2014. At BCN(TR) station NO_2 concentrations decreased from 54 to 38 μgm^{-3} (by 30%) while MAD(TR) station decreased from 60 to 32 μgm^{-3} (by 45%). The strong NO_2 concentration decrease observed at BCN(TR) and MAD(TR) reveals the important role of local/regional control measures in improving air quality with respect to NO_2. However, despite the large decrease observed in the last years in secondary NO_2 concentrations at BCN(TR) and MAD(TR) stations, the ambient NO_2 concentrations (around 50 μg m^{-3} at both stations in 2014) still exceding the NO_2 European annual standard limit and therefore more stringent control measures at local/regional level are still needed to comply with the standard limit established by the EU for this pollutant in both cities. These results highlight the significant impact of primary NO_2 emissions on the measured NO_2 concentrations in BCN(TR), MAD(TR) and GRA(TR), especially when compared with the threshold value for compliance with the European NO_2 annual limit of 40 μg m^{-3}. Since no drastic changes are expected in the after-exhaust treatment technology that can reduce primary NO_2 emissions to zero in the near future, and given that the secondary NO_2 concentrations constituted the large fraction of total ambient NO_2 measured in BCNTR, MADTR and GRATR (N70%), only a substantial reduction in NO_x emissions (and, therefore, in secondary NO_2 levels) will help to achieve lower NO_2 concentrations and comply with the European air quality standards.

2.2- CFD modeling of air quality in the city of Pamplona (Spain), assessment of health impacts

Fig 8: CFD modelling of annual average NO_2 and NO_x maps throughout an entire city (Rivas et al. 2019)

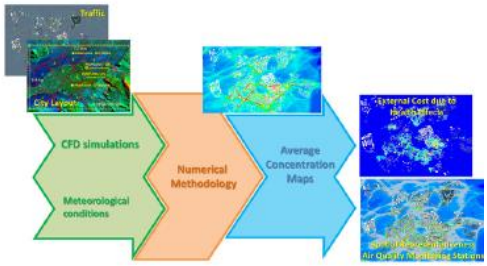

(a) (b)

A methodology based on CFD-RANS simulations (WA CFD-RANS, Weighted Averaged Computational Fluid Dynamic-Reynolds–Averaged Navier–Stokes simulations) which includes appropriate modifications, has been applied to compute the annual, seasonal, and hourly average concentration of NO_2 and NO_x throughout the city of Pamplona (Spain) at pedestrian level during 2016.

Urban air quality can be simulated by means of mesoscale models, however their spatial resolution (around 1 km^2) makes not possible to resolve the high pollutant gradients observed in the streets. Therefore, microscale models are necessary. Parameterized microscale models such as OSPM ((Berkowicz, 2000), SIRANE (Soulhac et al., 2011) or ADMS-URBAN (Di Sabatino et al., 2008) cited by Rivas et al. 2019) has been applied to simulate urban air quality. They are based on semi empirical assumptions about the relation between the flow and dispersion of pollutants, within and out of the streets, and the urban morphology. Nevertheless, CFD models solve momentum and transport equations around complex geometries, as urban environments. The advantage of CFD models versus parameterized models is their capability to deal with complex shaped walls or boundaries using flexible fine-scale grids.

The developed CFD methodology for this purpose makes possible to resolve hypothetical meteorological conditions using the existing CFD simulations, avoiding the handicap of the associated computational costs.

Table 4: Resume of principal information about the work by Rivas et al. 2019

Site	Sampling Model/method	Aim	Period
city of Pamplona (Spain)	CFD-RANS simulations. The results have been evaluated using measurements provided both by the city's network of air quality monitoring stations and by a network of mobile microsensors	obtain the annual and seasonal average concentration maps of NO_2 and NO_x and the time-evolution of the annual and seasonal averaged days at pedestrian level	2016

2.2.1- measured pollutant concentrations at air quality monitoring Stations

Table 4 Resume the principal information used in this study, In Fig 9 the comparison between PC, Rotxapea and Iturrama monitoring stations of the average daily evolutions of NO_x, NO_2, NO and O_3 concentrations for 2016 are shown. Two peaks of primary pollutant concentration (NO_x, NO_2 and NO) were observed, one at early morning (7 AM–8 AM local solar time) and another in the late afternoon (7 PM–8 PM)(Fig 9). As expected, higher concentrations were measured in the traffic station. These peaks were related to rush hour of traffic, photochemistry activity and planetary boundary layer (PBL) height. Unlike NO and NO_x, the late afternoon peak of NO_2 at the traffic station was higher than that recorded in the early morning,

probably due to a greater O_3 availability to produce NO_2 by titration (Leighton, 1961 cited by Rivas et al. 2019). After 8 AM, concentrations decreased until they reached their lower levels between 3 PM and 4 PM. As it is well known, O_3 concentrations are relatively low in the early morning, increase about midday and peak at around 3 PM, when the NO concentrations are low. The times for the maxima of nitrogen oxides were the result of the combination of high emissions from traffic during the rush hours with shallow mixing layers or low-height thermal inversion. Chemical reactions such as titration also play a significant role in increasing the NO_2 concentrations depending on the availability of O_3. Differences could be found between the summer and winter averages of the daily cycles of nitrogen oxides (Fig 9 b and c).

Fig 9: Average daily evolution of NO_x, NO, NO_2 and O_3 concentrations at monitoring stations for 2016: a) annual, b)winter and c) summer. Note that data of NO_2 and NO concentrations at Iturrama station were not available during 2016. (by Rivas et al. 2019)

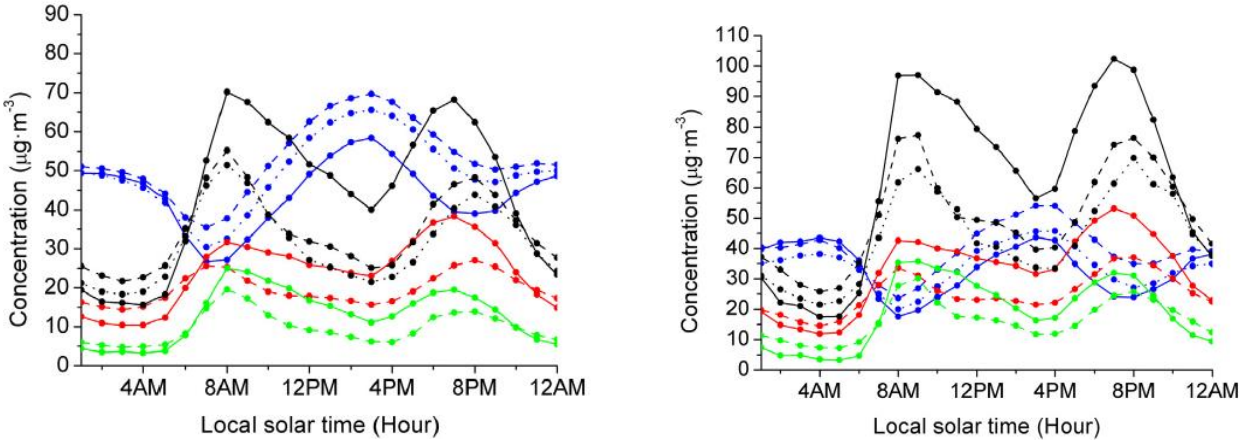

(a) (b)

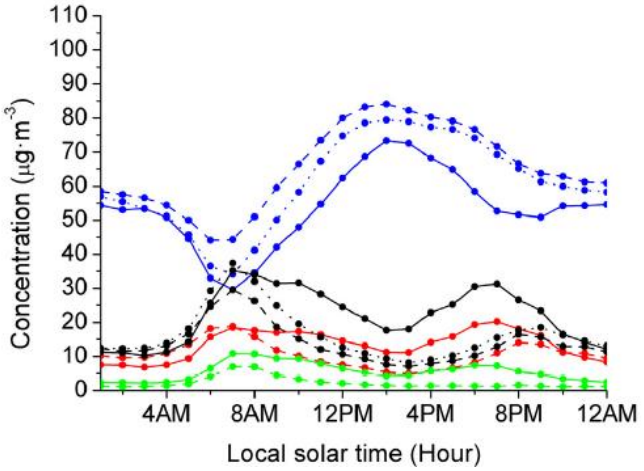

(c)

2.2.2- CFD model description

Fig 10 : Details of: a) CFD mesh model (buildings shaded in pink) and b) longitudinal plane section zoom and typical dimensions as function of the Zmax. (Rivas et al. 2019)

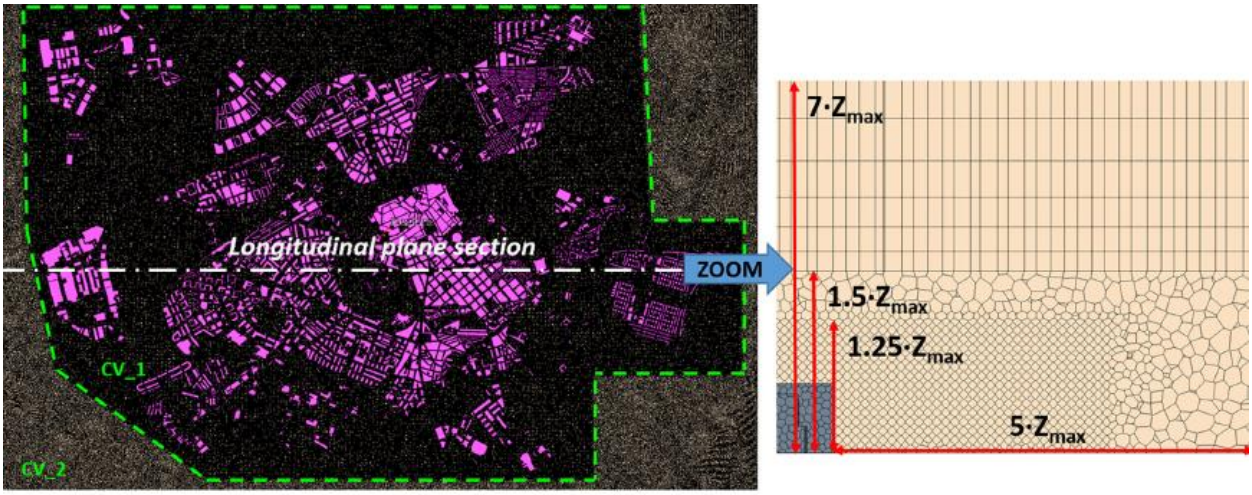

a) b)

Fig 11: topographic map of Pamplona's City and the 13 main neighbourhoods (limited by means of continuous red lines), GN, 2016, meteorological stations (green points), air quality monitoring stations (blue and yellow points, traffic and background stations respectively). (Rivas et al. 2019)

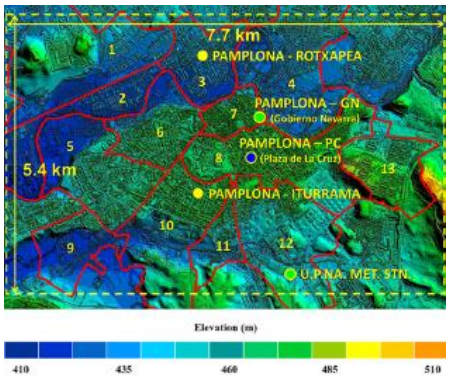

Table 5: Neighbourhoods characteristics of Pamplona (Rivas et al. 2019).

Number of neighbourhood	*Area* (km^2)	z_H (m)	Z_{max} (m)	λ_b (Adim.)
1	3.7	11	27	12
2	1.5	11	39	30
3	1.3	15	30	29
4	3.8	9	33	11
5	2.2	19	57	17
6	1.4	21	57	17
7	0.6	17	36	45
8	2.7	16	51	20
9	1.1	13	27	8
10	2.4	22	60	12
11	0.7	22	51	13
12	2.5	17	45	13
13	1.4	11	33	12

The numerical domain has about 42 Km^2(**Fig 11**), about 7.7 km × 5.4 km, and covers in excess the whole city (approx. 25.3 Km^2). A 3D full-scale geometrical model has been constructed, which considers the actual average height of each building separately.

The computational grid is a combination of polyhedral (between zH=

[0, 1.5 · Zmax], **Fig 10** b) and tetrahedral (between zH = [1.5 · Zmax, 7 · Zmax], **Fig 10** b) cells. The tetrahedral region is generated from the polyhedral core, as an extrusion in the direction zH, using a hyperbolic stretching law to compute the cell distribution growth in the direction of the extrusion (10 layers with a stretching

factor 1.3). This type of combination allows saving computational costs and is a good compromise when it comes to solving the atmospheric flow in the highest part of the domain. Instead, the polyhedral region is divided in two control volumes, CV_1(between zH = [0, 1.25 · Zmax], **Fig 10** b) and CV_2(between zH = [1.25 ·Zmax, 1.5 · Zmax], **Fig 10** b), whose typical resolutions are 5 m (in built-up zones) and 10 m (far from buildings) respectively, **Fig 10** a. In CV_1, the mesh includes further refinements in the narrowest streets and a prismatic layer of 1maround all urban surfaces (ground and buildings), to capture the influence of those obstacles. The transition between the prismatic layer and the core is carried out gradually, maintaining a growth factor of 1.3. The vertical and horizontal dimensions, **Fig 10** b, have been set following the recommendations given by Franke et al. (2007 cited by Rivas et al. 2019) and Di Sabatino et al. (2011 cited by Rivas et al. 2019). The total number of cells is 44.6 × 10*6.

In order to improve air quality, and meet the air quality standard limits in the European countries, the European Commission (EC) has implemented several stringent emission control measures along the last decades. Various EC control measures focused on vehicle emissions, such as EURO III, IV, V and VI emission standards, entered in force from 2000 to now on for restrictions of road traffic emissions, and 1999/32/EC for shipping emission restrictions. Numerical simulations are based on a steady state RANS approach with the Realizable k − ε Two Layer model. The commercial software STAR CCM+9.04.011® has been used (Siemens, 2018 cited by Rivas et al. 2019). To simulate the dispersion of primary pollutants inside the city, transport equations for passive scalars have been included, i.e., no chemical reactions of the primary pollutants are assumed. These equations consider both the advection and diffusion terms. And, the diffusivity is proportional to the turbulent viscosity (μt), computed by the Realizable k−ε model, and inversely proportional to the turbulent Schmidt number (Sct).

Therefore, the pollutant is assumed to be a passive scalar emitted by the traffic close to the ground in roads of the streets and avenues. The pollutant source at each road has been assumed as a proportional value to its Annual Average Daily Traffic, AADT (Fig. 10), and its length, and inversely proportional to the volume of the traffic emissions in such road. Then, CFD simulations do not provide the real concentrations but proportional values to real concentrations. In order to transform the computed values into real concentrations, a numerical methodology is applied.

Boundary conditions at buildings and ground surfaces are modelled considering the All Y+ wall hybrid treatment. Ground is considered a roughness wall with z0=0.05m. 16 different wind directions are simulated. Inlet profiles for wind speed are logarithmic and for turbulent kinetic energy (k) and turbulence dissipation rate (ε) are computed by the following equations (Richards and Hoxey, 1993 cited by Rivas et al. 2019):

$$U(z) = \frac{U^*}{k} \cdot ln\left\{\frac{(z+z_0)}{z_0}\right\}, k = \frac{{U^*}^2}{\sqrt{C\mu}}, \ \varepsilon = \frac{{U^*}^3}{k \cdot (z+z_0)} \quad \textbf{(4)}$$

where $u*$ is the friction velocity, z_0 is the roughness length, Cμ is a model constant (=0.09) and κ is von Karman's constant (κ = 0.4). For these simulations, $u*=0.24 m \cdot s^{-1}$ is used. This value indicates a velocity logarithmic profile at inlet with 3.2 $m \cdot s^{-1}$ at 10 m.

These neutral atmospheric conditions (isothermal conditions) are usually used in CFD simulations. In these conditions, simulated pollutant concentrations are inversely proportional to wind speed, however, $u*$ value has no influence in the final results because the WA CFDRANS methodology transforms simulated pollutant concentrations taken from CFD model at this velocity to modelled pollutant concentrations considering the measured wind speed. Several CFD-RANS studies have analysed the dependence of the pollutant concentration levels with the turbulent Schmidt number used in the turbulent mass transport equation. Typical values range from 0.7 to 0.9 (Delaunay, 1996; Baik et al., 2003 cited by Rivas et al. 2019), although Tominaga and Stathopoulos (2007 cited by Rivas et al. 2019) pointed out that the optimum values range from 0.2 to 1.3 depending on the geometry and flow properties. For the set of CODACS experiments, Vranckx et al. (2015 cited by Rivas et al. 2019) observed that the optimum Sct depended on the case and, in general, ranged from 0.3 to 1.0. Before this work, a sensitivity analysis about the turbulent Schmidt number has been carried out (not showed here). The optimal value for this case was 0.7, which agrees other works (Spalding, 1971; Li and Stathopoulos, 1997; Wang and McNamara, 2006 cited by Rivas et al. 2019).

2.2.3 - Methodology to estimate health effects

The estimation of the damage caused by air pollution required a complete methodological process known as the impact pathway developed in the framework of the Externe project series (Bickel and Friedrich, 2005 cited by Rivas et al. 2019).

This methodology offers an analytical framework capable of transforming the information related to the emission of different pollutants into a common unit: monetary units. The process consists in following the pollutants throughout all the phases, from their emission until they reach the receptors, causing them damage. The following stages can be distinguished:

a. Emission of pollutants.

b. Atmospheric concentration: estimating the concentrations of pollutants in the area of study.

c. Exposure of the population to the concentrations of NO_2 produced. A requirement is knowing the spatial and age distribution of the city's population.

d. Environmental impact. The estimation is carried out through the application of exposure-response functions that allow determination of the increase in the health endpoints caused by an increase in the atmospheric concentration of the pollutant.

e. Damage caused, which consists in estimating the value that the population attributes to the impacts caused by pollution. This estimation allows determining the deterioration of the wellbeing of the population because of the variation in the atmospheric quality induced by the pollution emitted by road traffic in the urban environment.

We followed the above methodology using the NO_2 concentration maps obtained through our modelling; the data of the Municipal Census of Inhabitants as the age-specific distribution of the population of the city of Pamplona in a grid of 100 × 100 m cells; and information from the literature about the incidence of diseases related to exposure to NO_2.

The health impacts were quantified through the exposure-response functions proposed by the World Health Organization (WHO, 2013b cited by Rivas et al. 2019), by applying the following formula to each cell in the domain:

$$\boldsymbol{I = C \times P \times R \times CRF \times V} \quad \textbf{(5)}$$

Where,

I: Impact expressed as number of additional cases

C: Concentration of the pollutant
P: Population at risk
R: Incidence ratio
CRF: Concentration Response function or change in incidence per unit of concentration
V: Monetary valuation of the impact on health.

The exposure concentration response functions used were those proposed by the WHO in the HRAPIE project (WHO, 2013b cited by Rivas et al. 2019):

1) Effects of long-term exposure to NO_2 on mortality in the population over 30 years of age. The WHO experts recommend the application of a linear CRF function that corresponds to a relative risk (RR) of 1.055 (confidence interval 1.031–1.08) for every 10 μg·m³ of annual mean concentration of NO_2. This RR value was obtained from a meta-analysis by Hoek et al. (2013 cited by Rivas et al. 2019) and considers a threshold concentration of 20 μg·m³. The mortality rate was obtained from the Statistical Institute of Navarra for the entire province of Navarra and was 0.89% for the year 2015 (NA-STAT, 2018 cited by Rivas et al. 2019).

2) Effects of long-term exposure to NO_2 on the onset of bronchitis symptoms in asthmatic children between ages 5 and 14. The WHO recommends the use of the results of McConnell et al. (2003 cited by Rivas et al. 2019), which calculate a RR of 1.021 (confidence interval 0.99–1.06) for every 1 μg·m³ of NO_2. The percentage of asthmatic children in the city of Pamplona was obtained from the data of the Primary Care Service of the Navarra Health Service for each of health district of the city. The prevalence of bronchitis symptoms in asthmatic children was considered as the average of the values in Migliore et al. (2009) and McConnell et al. (2003) (cited by Rivas et al. 2019), being 21.1% and 38.7% respectively.

3) Effects of short-term exposure to increased levels of NO_2 in mortality. WHO recommends using the results of the APHEA-2 project (Samoli et al., 2006 cited by Rivas et al. 2019) covering 30 European cities and obtaining

an RR value of 1.0027 (confidence interval 1.0026–1.0038) for every 10 μg·m3 of daily maximum 1 hour mean maximum concentration of NO_2.

4) Effects of short-term exposure to increased concentrations of NO_2 in hospital admissions for respiratory diseases. The WHO recommends the use of RR values from the study by Anderson et al. (2007 cited by Rivas et al. 2019) of 1.018 (confidence interval 1.0115–1.0245) per 10 μg·m³ of average 24-hour mean daily maximum concentration. The base value for hospital admissions for respiratory diseases was obtained from the WHO European Hospital Morbidity Database (WHO, 2013a cited by Rivas et al. 2019) and is 1.26% for Spain.

2.3- the effect of short-term of NO_2 on daily mortality in Spanish cities

Table 6: Resume of principal information about the work by Linares et al. 2018.

Site	Sampling Method	Aim	Period
Spanish	estimate RRs and ARs, we used generalised linear models with a Poisson link, controlling for maximum and minimum daily temperature, trend of the series,ol'[seasonalities, and the autoregressive nature of the series. A meta-analysis with random effects was used to estimate RRs and ARs nationwide.	quantify the relative risks (RRs) and attributable risks (ARs) of daily mortality associated with NO_2 concentrations recorded in Spain and calculate the number of NO2-related deaths.	2000–2009

Ambient air pollution was a leading risk factor for the global disease burden in 2015, and its contribution remained relatively stable from 1990 to 2015 (GBD, 2015 cited by Linares et al. 2018). The US Environmental Protection Agency, the World Health Organisation (WHO), and a number of literature reviews have shown that long- and short-term exposure to ambient air pollution increases mortality and morbidity due to cardiovascular diseases, respiratory diseases and lung cancer, and shortens life expectancy (Cohen et al., 2017 cited by Linares et al. 2018). Motor vehicles are the most significant source of urban air pollution. $PM_{2,5}$ is the air pollutant whose health effects have been most closely studied (Basagaña et al., 2015

cited by Linares et al. 2018), and is the variable most commonly used as a proxy indicator of exposure to air pollution, whereas evidence on NO_2 concentrations is still under study. There are several reasons for this but; in essence, it is more difficult to judge the independent effects of NO_2 in studies because, in such research, the correlations between concentrations of NO_2 and other pollutants are often high, so that NO_2 might actually be representing a mix of traffic-related air pollutants.

At this point in time, this fact is particularly important in Europe, since NO_2 concentrations have not been decreasing at the same pace as PM emissions (probably reflecting the impact of the Euro 4 and 5 vehicle standards on reducing diesel PM). This change in ratio has implications for the interpretation of NO_2 as a quantitative proxy for PM vehicle pollution, and highlights the need to understand the effects of NO_2 per se. Moreover, in Spain -the country which is the focus of this study- statutory and WHO guideline values are currently being complied with in the case of PM but not in that of NO_2.

In Spain, the Spanish Multicentre Study on the Relationship between Air Pollution and Mortality (Estudio Multicéntrico Español sobre la Relación entre la Contaminación Atmosférica y la Mortalidad/EMECAM) (cited by Linares et al. 2018) analysed data on atmospheric concentrations of black smoke, SO_2,, NO_2, CO and O_3, temperature and other aspects in 14 Spanish cities, and reported the existence of an association between NO_2 and cardiovascular and all-cause mortality, though based on data from only 7 and 3 cities respectively. The studies undertaken to date in Spain linking NO_2 exposure to short-term mortality have been rendered obsolete by the fact that they were based on information which dated from the beginning of the 1990s and included only a few cities due to the lack of monitoring data, with no study having yet been conducted that includes all of the country's provinces. This study therefore set out to update the impact of daily mean NO_2 concentrations on population mortality at a national level.

2.3.1- Variables used in the study

Used daily mean NO_2 concentrations measured in μg/m³ as the measure of mean population exposure to this pollutant. The readings, as supplied by the Ministry of Agriculture & Environment (*Ministerio de Agricultura, Alimentación y Medio Ambiente/MAGRAMA*), were taken across the period 2000–2009 at monitoring

stations, which, according to available data, were validated mainly for urban traffic and were situated in each provincial capital. All the monitors used were of urban type and placed in the capital of the province. When there is more than one station, was calculate the mean of the total monitors. In case of lack of data in one monitor, the missing values were calculated through the rest of the monitors. As the dependent variable, It used daily mortality due to natural (all causes except accidents) (International Statistical Classification of Diseases and Related Health Problems, 10th Revision (ICD-10): A00- R99), circulatory (ICD-10: I00-I99) and respiratory causes (ICD-10: J00- J99) registered in 52 Spanish provinces across the period 2000–2009. In the case of Madrid, the data corresponded exclusively to the Madrid metropolitan area, and were not provincial in scope. These data were furnished by the National Statistics Institute (*Instituto Nacional de Estadística/INE*).

As control variables, it used different variables related to the designated study objective, namely:

Accordingly, the aim was: to analyse the short-term association between NO_2 concentrations and all-cause, circulatory-cause and respiratory- cause mortality in all Spanish provinces; and to update the impact and attributable mortality in the country as a whole.

- Daily mean PM_{10} concentrations (μg/m³), measured at the same stations as those which obtained the NO_2 values, and likewise supplied by the MAGRAMA.
- Maximum temperatures (Tmax) and maximum temperatures (Tmin) at each reference observatory situated in each provincial capital. These data were furnished by the State Meteorological Agency (Agencia Estatal de Meteorología/AEMET).
- We controlled for the presence or absence of influenza epidemics. This variable was introduced dichotomously, with a value=1 when there was an epidemic and a value=0 when there was no epidemic. This information was supplied by the National Centre of Epidemiology (Carlos III Institute of Health).
- Trend of the series and annual, six-monthly, four-monthly and three monthly seasonalities were taken into account, using the sine and cosine functions of the periods of 365, 180, 120 and 90 days respectively. In addition it also controlled for the autoregressive nature of the dependent variable.

2.3.2- Impact models

To quantify the impact of daily mean NO_2 concentrations on mortality, constructed generalised linear models (GLMs) with the Poisson regression link, with appropriate control for overdispersion (negative binomial). Bipollutant models (NO_2 andPM_{10}), when it was possible, have been performed. In these models, as indicated above, included the parametrized variables along with their corresponding lags. The procedure used to determine significant variables was «Backwards-Step», beginning with the model that included all the explanatory variables and gradually eliminating those which individually displayed least statistical significance, with the process being reiterated until all the variables included were significant at $p < 0.05$. This methodology makes it possible to calculate the relative risks (RRs) associated with given increases in the significant independent variables, so that in this case the RRs were calculated for every 10 μg/m³ increase in NO_2 concentrations.

RRs were calculated for natural-, circulatory- and respiratory cause mortality in each province. The RRs for each province yielded by the Poisson regression models were combined by means of a meta-analysis of random effects, which incorporates an estimate of inter-study variability (heterogeneity) in the weighting (Sterne, 2009 cited by Linares et al. 2018), thereby obtaining a measure of the RR (95% CI), not only at an Autonomous Region level, but also at that of all the provinces which proved to be statistically significant.

2.3.3- Attributable mortality

To ascertain the number of deaths attributable to NO_2 concentrations in each province shown to be statistically significant, used the methodology published in Tobías et al., (2015 cited by Linares et al. 2018). This methodology is based on the fact that the previously calculated value of the attributable risk (AR) represents the percentage increase in daily mortality for every 10 μg/m³ increase in the pollutant studied. The population attributable risk (AR) is calculated based on the RR associated with this same increase, via the following equation:

$AR=((RR-1) / RR)\times100$ (Coste and Spira, 1991 cited by Linares et al. 2018).

The percentage increase in daily mortality associated with a given concentration is thus calculated by multiplying it by this AR and dividing by 10. The number of daily deaths attributable to this concentration is then obtained by multiplying this percentage increase in mortality by the number of daily deaths, and

dividing by one hundred. In this way, the mortality associated with the concentration of this pollutant (in this case, NO_2) in a given town/city can be calculated for each day.

Finally, to estimate the percentage of attributable mortality due to annual NO_2 concentrations above the WHO recommendations has been calculated considering annual mean with NO_2 concentrations above 20 μg/m³. This value represent half of the current guideline value of WHO.

The computer software programmes used for all statistical analyses were IBM SPSS Statistics 22 and STATA v 14.1.

2.3.4- Results

The overall RRs obtained for Spain, corresponding to increases of 10 μg/m3 in NO_2 concentrations were 1.012 (95% CI: 1.010 1.014) for natural-cause mortality, 1.028 (95% CI: 1.019 1.037) for respiratory-cause mortality, and 1.016 (95% CI: 1.012 1.021) for circulatory-cause mortality. This amounted to an annual overall 6085 deaths (95% CI: 3288 9427) due to natural causes, 1031 (95% CI: 466 1585) due to respiratory causes, and 1978 (95% CI: 828 3197) due to circulatory causes.

2.4-exposure to air pollution in relation to socio-economic indicators in European metropolitan areas

A limited number of studies have addressed environmental inequality, using various study designs and methodologies and often reaching contradictory results. Following a standardized multi-city data collection process within the European project EURO-HEALTHY, we conducted an ecological study to investigate the spatial association between nitrogen dioxide (NO_2), as a surrogate for traffic related air pollution, and ten socioeconomic indicators at local administrative unit level in nine European Metropolitan Areas.

Mixed models was apply for the associations under investigation with random intercepts per Metropolitan Area, also accounting for the spatial correlation. The stronger associations were observed between NO_2 levels and population density, population born outside the European Union (EU28), total crimes per 100,000 inhabitants and unemployment rate that displayed a highly statistically significant trend of increasing concentrations with increasing levels of the indicators. Specifically, the highest vs the lowest quartile of each indicator above was associated with 48.7% (95% confidence interval (CI): 42.9%, 54.8%), 30.9% (95%CI: 22.1%, 40.2%), 19.8% (95%CI: 13.4%, 26.6%) and 15.8% (95%CI: 9.9%, 22.1%) increase in NO_2 respectively.

The association with population density most probably reflects the higher volume in vehicular traffic, which is the main source of NO_2 in urban areas. Higher pollution levels in areas with higher percentages of people born outside EU28, crime or unemployment rates indicate that worse air quality is typically encountered in deprived European urban areas. Policy makers should consider spatial environmental inequalities to better inform actions aiming to lower urban air pollution levels that will subsequently lead to improved quality of life, public health and health equity across the population.

Fig 12: Metropolitan areas included in the study. (Samoli et al. 2019)

2.4.1- Data and methods used

Collected data on environmental and socioeconomic indicators in the framework of the European project EURO-HEALTHY that aimed to characterize health equity across Europe using a standardized protocol procedure under an ecological study design. Data were collected at a comparable administrative spatial level, roughly corresponding to municipalities. Following the EUROSTAT's hierarchical system of Local Administrative Units (LAU) focal points from each MA collected the data for one of the following levels: the upper LAU level (LAU level 1) and the lower LAU level (LAU level 2). For most European countries, LAU-2 corresponds to municipalities (Sohn and Stambolic, 2013 cited by Samoli et al. 2019). Therefore, collected data at municipality level for nine MA across Europe for the period 2001-14 (Fig 12) considering the following LAU level: Athens, Greece, including 40 LAU 1; Barcelona, Spain, including 23 LAU 2; Berlin- Brandenburg,

Germany, including 23 LAU 1; Brussels, Belgium, including 91 LAU 2; Lisbon, Portugal, including 18 LAU 1; London, UK, including 33 LAU 1; Paris, France, including 150 LAU 2); Stockholm, Sweden, including 26 LAU 2 and Turin, Italy, including 49 LAU 2.

For the present analysis, considered SES indicators with available data from at least five MA in 2001 - 14. These are presented and included: unemployment and youth (aged 15 - 24 years old) unemployment rate, disposable income of private households per capita, number of crimes per 100,000 inhabitants, population aged 25 - 64 with upper secondary or tertiary education attainment, early leavers from education and training and population born in non EU28 countries. further considered daily smokers aged above 15 years and population density as indirect SES indicators and finally the area's ageing index as an indicator of the health susceptibility and vulnerability of the population. Different MA collected data for different years, within the period 2001 - 14, depending on the indicator and its availability from the census or other sources of data, such as police records (for crimes) and representative population surveys (for smoking prevalence data). Furthermore, some indicators were provided annually, while others in 3- and 4-years intervals. considered indicators that were available for the period 2010 - 14 in order to have a time correspondence with NO_2 data availability but also because data for this period were more complete compared to previous years. When indicators were provided annually, we assigned to each LAU the average of the indicator's levels for the available years within 2010 - 14. In cases that an indicator was not available at LAU level, the value of an upper administrative level was assigned to all LAUs within that city for descriptive purposes but the MA was excluded from further analysis of the specific variable (as was the case for the income and crimes indices in Athens, or percent of daily smokers in Paris).

Initially performed the analysis separately by MA. And then calculated the Spearman correlation coefficients between NO_2 and SES indicators and applied linear regressions, accounting for each indicator separately. Estimated the spatial autocorrelation of the residuals by Moran's I to assess model assumptions (Havard et al. 2009 cited by Samoli et al. 2019). In the second stage of the analysis, data from all MA were pooled and analyzed together by applying mixed models for the associations under investigation with random intercepts per MA and accounting for the spatial correlation by the introduction of a bivariate thin plate regression spline

for the centroid's geographic coordinates of each LAU, as implemented by Wood (2003 cited by Samoli et al. 2019). In all analyses NO_2 was log-transformed as its original distribution deviated from the normal. The indicators were entered in the models one at a time using MA specific quartiles to account for linearity deviations. We tested the sensitivity of our findings by using quartiles for the indicators as estimated by the overall distribution across the 9 MA, acknowledging as drawback in this analysis that in the overall distribution different MA contribute to different levels.

Finally assessed the consistency of the associations in models adjusting for population density.

2.4.2- Results

All cities except London, the highest correlation across the indicators was observed with population density, ranging from 0.70 in Turin to 0.96 in Berlin Brandenbourg. In London the highest correlation was observed with the crime rate (r = 0.85). Negative correlations were also observed, which were especially high in Berlin-Brandenbourg for the association with income (r=0.69) and population aged 25-64 years with upper secondary or tertiary education (r=0.68). MA-specific linear regression models indicated low to moderate spatial autocorrelation for the great majority of the indicators, ranging from 0.07 in Athens for most indicators to 0.42 in Brussels for the association with the aging index. In all analyses, addressed this spatial autocorrelation by adding a smooth bivariate term for each municipality's geographic coordinates in the mixed models analysis with the pooled data over all MAs. All indicators presented positive associations with NO_2 concentrations indicating increases for levels above the lowest quartile of the indicator distribution. Among the indicators analyzed, the stronger associations were observed between NO_2 levels and population density, population born outside the EU28, crimes per 100,000 inhabitants, and unemployment rate, which displayed a highly statistically significant trend of higher NO_2 concentrations with increasing levels of the indicators. Specifically, the highest vs the lowest quartile of each of these four socioeconomic indicators was associated with 48.7% (95% confidence interval (CI): 42.9%, 54.8%), 30.9% (95%CI: 22.1%, 40.2%), 19.8% (95%CI: 13.4%, 26.6%) and 15.8% (95%CI: 9.9%, 22.1%) increase in NO_2 respectively. A statistically significant increasing trend was observed for areas with a higher ageing index, where

the areas at the highest quartile of the ageing index had 11.9% higher NO_2 levels. The association with youth unemployment rate and the percentage of smokers over 15 years indicated that the middle levels of the indicators presented the highest increases in NO_2 levels, rather than the highest. Income and higher education attainment indices were not significantly associated with NO_2 levels. The models using pooled data quartiles for the indicators identified the same statistically significant indicators that followed the same patterns as in the analysis with the MA-specific quartiles, while the magnitude of the effects increased in all cases except for the population born in non EU28 (decreased) and the ageing index (identical). Models adjusting for population density also revealed the same patterns although the magnitude of the effects decreased.

2.5- the health effects of exposure to physical and chemical properties of airborne particles

Table 7: Resume of principal information about the work by Pirani et al. 2015

Site	Sampling Method	Aim	Period
London (UK)	Dirichlet process mixture models	cluster time points with similar multipollutant and response profiles, while adjusting for seasonal cycles, trends and temporal components.	2002–2005

Airborne particles are a complex mix of organic and inorganic compounds, with a range of physical and chemical properties. Estimation of how simultaneous exposure to air particles affects the risk of adverse health response represents a challenge for scientific research and air quality management. In this paper, we present a Bayesian approach that can tackle this problem within the framework of time series analysis.

To gain better insight into the features of air pollution mixtures and their effect, there is a consequent need to explore new statistical methods able to integrate standard methodological tools for a better understanding of these complex systems. In a recent review of techniques for estimating health effects of multiple air pollutants.

2.5.1- Measurements of PM and Data of Mortality

Daily average concentrations of particle metrics included: particle number concentration (PNC), inorganic anions such as chloride, nitrate and sulphate, black smoke (BS) and gravimetric measurements of PM, such as PM_{10}, $PM_{2.5}$ and PM

coarse fraction (that is, $PM_{10-2.5}$ obtained by subtraction). With the exception of BS, the daily concentrations were obtained from a single background monitoring station in central London (North Kensington). BS was an average across several urban and suburban stations. PNC was measured using a TSI 3022A condensation particle counter, where particles are enlarged by condensation of saturated butanol vapour which are then counted using a laser and optical detector. The PM_{10} 24-hour filter samples were collected at 16.7 l per minute on quartz fibre filters using Partisol 2025 (Thermo) instruments and these filters were analysed by ion chromatography. Finally, daily average gravimetric PM_{10} and $PM_{2.5}$ were sampled using a Partisol sampler and measured using methods in EN12341 and EN14907.

The data set also included PM apportioned into primary and nonprimary sources (Fuller et al., 2002; Fuller and Green, 2006 cited by Pirani et al. 2015), giving modelled primary PM_{10} (P PM_{10}), and non-primary PM subdivided by size fraction: non primary PM_{10} (NP PM_{10}), non-primary $PM_{2.5}$ (NP $PM_{2.5}$), and non-primary PM coarse fraction (NP coarse). The source apportionment model assumed that primary PM_{10} was associated with nitrogen oxide (NO_x) sources and the non-primary component was the fraction of PM not associated with NO_x. NO_x is generally considered a robust marker for traffic pollution.

To better quantify the average health impact of these particles, was measured the same set of metrics in 2012, and computed and compared the posterior predictive distributions of mortality under the exposure scenario in 2012 vs 2005.

For the year 2012, the PM measurements (except BS) were collected at the same background monitoring station in central London. Between 2005 and 2012, gravimetric filter substrates were changed from quartz fibre to PTFE coated glass fibre (Emfab, Pall). Because BS is no longer measured in London, daily mean of BS was computed from equivalent measured black carbon by aethalometer (Magee Scientific) at two background monitoring sites, and applied an adjustment factor of 0.27 following Heal and Quincey (2012 cited by Pirani et al. 2015).

Daily count of deaths from respiratory diseases of London residents (2002 2005) were obtained from the Office for National Statistics and coded using the International Classification of Diseases, 10th Revision (ICD-10: Chapter J).

2.5.2- Profile regression model for time series of multiple particles and health

The data of exposure were normalised to be on a comparable scale adopting the modified z-score recently proposed by Austin et al. (2012 cited by Pirani et al. 2015) Let $x_{t,p}$ be the measurement on day t of particle metric p, for t = 1,…,T and p = 1,…,P. transformed the original measurements as $z_{t,p}$ = ($x_{t,p}$ − Median(x_p))/(Median(|$x_{t,p}$− Median(x_p)|)).

In the previous analysis, observed associations for respiratory mortality with 1–day lag secondary PM masses. The estimated regression coefficients were obtained fitting separate univariate log-linear Poisson models. To study the value added by this new approach, it was considered the previous study of Atkinson et al. (2010 cited by Pirani et al. 2015) as benchmark and thus the 1day lag was chosen as the exposure window for particles.

The proposed model is based on the DP, a popular tool for Bayesian nonparametric analysis, which relies on mixtures to represent distributions in the data. Symbolize by t=1,…,T a series of temporal points. Let the data consist of realizations of a response data vector y = (y_1,…,y_T), a set of (normalised) covariates (i.e., predictors) $z_{t,p}$, p=1,…,P, and a collection of confounding factors $u_{t,h}$, h=1,…,H. In this study, yt denotes the count number of deaths for respiratory diseases on day t, z_t=(z_t,1,…, z_t,P)′ represents a daily covariate profile of air particles, and u_t=(u_t,1,…, u_t,H)′ is a B-spline basis matrix for natural cubic splines of calendar time and temperature.

Assumed a joint probability model for the data, which takes the following form:

$$P(y_t, z_t|\Theta, u_t) = \sum_{k=1}^{\infty} w_k \, p(y_t|\Theta_k, \Theta_0, u_t)p(z_t|\Theta_k, \Theta_0) \qquad (6)$$

where w_k are the mixture probabilities satisfying $\sum_{k=1}^{\infty} w_k = 1$ almost surely and indicating the probability of belonging to the kth component. Θ denotes the collection of model parameters, that includes component specific parameters Θ_k, and global parameters Θ_0, that is, Θ = (Θ_k, Θ_0).

The inference for such mixture models can be simplified by introducing latent variables that indicate the group memberships of objects (i.e., the cluster to which day t belongs to). These latent group labels define as: g = (g_1,…, g_t), such that p (g_t = k) =w_k. Thus, g_t is chosen using a multinomial distribution parameterised by the mixing probabilities, g_t|w ~ Multinomial(w).

Rather than specifying a parametric distribution for the mixture probabilities, w_k, modelled them as unknown quantities to be estimated by the data. Specifically, assumed that w_k are generated using a stick breaking representation of the DP given by Sethuraman (1994 cited by Pirani et al. 2015). The name of this construction derives from an analogy given by breaking pieces off from a stick of unit length, where the breakpoints are randomly sampled from the Beta distribution. The mixture probabilities break the stick into a potentially infinite number of pieces, such that $\sum_{k=1}^{\infty}$ wk = 1 . The first mixture probability is equal to V1, i.e., w1=V1, where V1 ~ Beta(1,α) and for k ≥ 2 the k -th mixture probabilities are given by $V_k \Pi_{i=1}^{k-1}(1 - Vi)$. A Gamma distribution was used to specify prior uncertainty for the precision parameter of DP (following Escobar and West (1995)) (cited by Pirani et al. 2015), namely α ~ Gamma(a,b), where a = 2 and b = 1 are the shape and the inverse scale (rate) parameter respectively.

A multivariate normal distribution was assumed for the P covariates:

$$p(z_t|\,\Theta_k,\Theta_0) = (2\Pi)^{-\frac{p}{2}}|\Sigma_k|^{-\frac{1}{2}}\exp\left\{-\frac{1}{2}\,(z_t - m_k)'\,\Sigma_k^{-1}(z_t - m_k)\right\} \qquad \textbf{(7)}$$

where m_k = ($m_{k,1}$,…,$m_{k,p}$) is the mean vector for component k (i.e., location parameters), and Σ_k is the P × P symmetric positive definite variance covariance matrix.

Specified hyperpriors for m_k and Σ_k similar to Molitor et al. (2011 cited by Pirani et al. 2015), adopting an empirical Bayesian approach. A normal distribution was assumed for the location parameters, that is, m_k ~ N(m_0, Σ_0) (with m_0 equal to the empirical mean of each covariate, and Σ_0 having a diagonal structure with elements equal to the square of empirical range of each covariate). specified a Wishart distribution for the precision matrix $Q_k = \sum_k^{-1}$ (i.e., inverse variance–covariance matrix), that is, Q_k ~W(Φ,ν), where Φ is a symmetric (non-singular)

matrix parameter (set equal to the inverse of the empirical variance multiplied by 1/P) and v is the degrees of freedom parameter (set equal to P).
The response was modelled as a Poisson:

$$P(y_t|\Theta_k, \Theta_0, u_t) = \frac{\lambda_t^{y_t}}{y_t!} exp(-\lambda_t) \quad \textbf{(8)}$$

where

$$\lambda_t = E_t \, exp(u_t) \quad \textbf{(8.1)}$$

and

$$\mu_t = \mu_k + \sum_{h=1}^{H} f_h\left(U_{t,h}, df_h\right) + \varepsilon_t \quad \textbf{(8.2)}$$

assuming ε_t be normal distributed with zero mean and variance σ_ε^2. Here μ_t is the mean response for day t and E_t is the expected offset given by the average number of deaths for respiratory diseases in the full period in study.

The parameter of interest is μ_k, which represents the log relative risk for the outcome of interest associated with the kth cluster, were each cluster includes days with similar multipollutant profile. The functions f($\cdot$,df_h) denote smooth functions of confounding factors, with smoothing parameters df_h. The basis functions are associated with the relative coefficientsβ_1,…,β_H, that assumed follow a weakly informative Student-t prior distribution, with location, scale and degree of freedom set to 0, 2.5 and 7 respectively, that is $\beta \sim t_7(0,2.5)$.

2.5.3- Results

Precis statistics for deaths for respiratory-related diseases and ambient air particles measured in London in the period shown in table 7 are given in Table 8.

The correlations between the daily concentrations of pollutants showed different degrees of interdependence in these metrics, as shown in Table 9.

The representative clustering separated the days into three main clusters, which included respectively 1156, 63 and 242 days. Fig.13 shows the posterior

distributions for the particle metrics by cluster, while Table 10 displays a summary of the cluster multipollutant profiles on their original scale.

Table 8: Descriptive statistics of respiratory mortality and airborne particle metrics. London, 2002–2005.(Pirani et al. 2015)

Variables	Mean	Range	Percentiles		
			25th	50th	75th
Deaths (per day)	21.60	6.00–58.00	16.00	21.00	26.00
PNC (cm^{-3}/1000)	21.19	5.39–52.44	14.63	19.97	25.91
PM component					
Chloride ($\mu g/m^3$)	1.31	0.01–9.06	0.25	0.88	1.98
Nitrate ($\mu g/m^3$)	3.77	0.03–30.89	1.35	2.44	4.47
Sulphate ($\mu g/m^3$)	2.93	0.23–20.63	1.51	2.25	3.89
BS ($\mu g/m^3$)	6.23	1.40–31.33	4.00	5.40	7.60
PM size					
PM_{10} ($\mu g/m^3$)	26.63	5.00–119.00	17.00	23.00	32.00
$PM_{2.5}$ ($\mu g/m^3$)	18.85	1.00–104.00	11.00	15.00	22.00
Coarse ($\mu g/m^3$)	7.89	0–33.00	5.00	7.00	10.00
PM source apportionment					
PPM_{10} ($\mu g/m^3$)	4.63	0.80–39.10	2.50	3.70	5.60
$NPPM_{10}$ ($\mu g/m^3$)	11.50	0–61.00	7.00	9.90	14.20
$NPPM_{2.5}$ ($\mu g/m^3$)	5.75	0–32.60	2.40	4.20	7.40
NPcoarse ($\mu g/m^3$)	5.99	0–42.20	4.00	5.60	7.40

Table 9: Correlation between pairs of airborne particle metrics. London, 2002–2005. (Pirani et al. 2015)

	PNC	Chloride	Nitrate	Sulphate	BS	PM_{10}	$PM_{2.5}$	Coarse	PPM_{10}	$NPPM_{10}$	$NPPM_{2.5}$	NPcoarse
PNC												
Chloride	0.34											
Nitrate	0.38	−0.17										
Sulphate	0.08	−0.31	0.52									
BS	0.49	−0.16	0.46	0.35								
PM_{10}	0.30	−0.16	0.67	0.66	0.48							
$PM_{2.5}$	0.31	−0.29	0.70	0.68	0.51	0.91						
Coarse	0.09	0.11	0.18	0.25	0.13	0.57	0.26					
PPM_{10}	0.72	−0.09	0.53	0.30	0.74	0.53	0.56	0.15				
$NPPM_{10}$	−0.12	−0.16	0.43	0.55	0.20	0.68	0.60	0.49	0.11			
$NPPM_{2.5}$	−0.16	−0.39	0.48	0.68	0.28	0.67	0.68	0.31	0.14	0.86		
NPcoarse	0.02	0.22	0.21	0.15	0.03	0.43	0.25	0.56	0.06	0.71	0.31	

Compared to clusters 1 and 3, cluster 2 had larger posterior errors as the number of days included was lower. The risk of mortality for respiratory diseases varied according to these cluster profiles.

Cluster 1 was characterized by low posterior estimates for most of the particles (except chloride), and had the lowest risk of mortality when compared to the average mortality in 2002 - 2005. The posterior relative risk of mortality, μ_1, associated with this cluster was 0.98 (95% credible intervals (CI): 0.96,1.00).

Cluster 2 was characterized by low posterior estimates of inorganic anions and secondary particles and higher posteriors for primary emissions, with a posterior relative risk of mortality, μ_2, equal to 1.00 (95% CI: 0.97, 1.03). This cluster included mainly winter days.

Finally, cluster 3 was dominated by secondary aerosol, especially nitrate and sulphate, with high posteriors of non-primary airborne particles. Found a posterior relative risk of mortality, μ_3, equal to 1.02 (95% CI: 1.00, 1.04). This third cluster included mainly spring and autumn days.

Fig. 14 displays the heatmap of the posterior probabilities that the days (period: 2002–2005)(table 7) were included in a cluster. For this data set, It was found that the days exhibited a high probability of being assigned to a specific cluster.

Also it was analysed the posterior estimates for the coefficients associated with the design matrices of B-splines of time and temperature for controlling for seasonal and long-term trend and weather conditions. The posterior mean and the 95% CI of the estimated coefficients are displayed in Fig. 15, showing the effective capability of the model to depict the non-linear effect of these factors.

Fig 13: Box plots showing the distribution of the posteriormeans for each particle component (on normalised scale) for the three clusters that form the representative clustering (A = cluster 1; B = cluster 2; C = cluster 3). (Pirani et al. 2015)

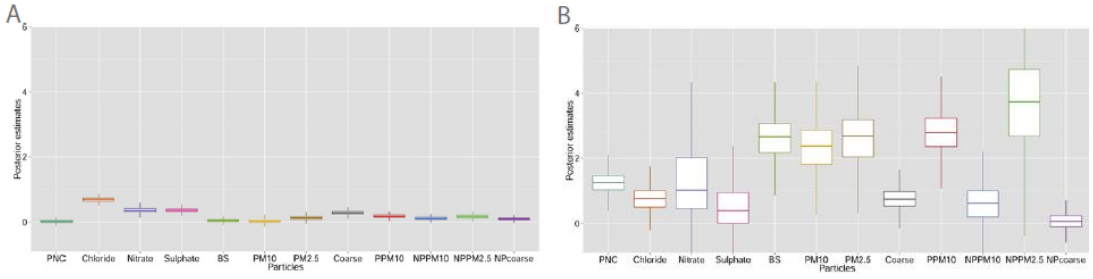

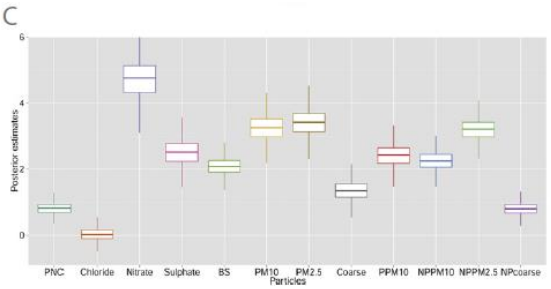

Table 10: Summary of cluster profiles (on original scale): distribution means (95% CI) for characteristics of clusters from the representative clustering. (Pirani et al. 2015)

Particle compounds	Cluster 1 (1156 days)	Cluster 2 (63 days)	Cluster 3 (242 days)
PNC (cm^{-3}/1000)	20.08 (19.54, 20.67)	27.01 (23.63, 30.42)	24.56 (22.58, 26.51)
Chloride ($\mu g/m^3$)	1.38 (1.28, 1.47)	1.43 (0.95, 1.90)	0.90 (0.62, 1.21)
Nitrate ($\mu g/m^3$)	2.90 (2.73, 3.41)	3.76 (2.19, 7.74)	8.58 (6.49, 9.90)
Sulphate ($\mu g/m^3$)	2.61 (2.49, 2.79)	2.65 (1.73, 4.54)	4.76 (3.94, 5.50)
BS ($\mu g/m^3$)	5.48 (5.33, 5.76)	9.80 (7.59, 11.57)	8.83 (7.65, 9.82)
PM_{10} ($\mu g/m^3$)	23.16 (22.51, 25.48)	37.24 (26.94, 45.09)	42.52 (37.61, 47.25)
$PM_{2.5}$ ($\mu g/m^3$)	15.65 (15.12, 17.40)	28.45 (19.10, 35.12)	32.09 (26.84, 35.82)
Coarse ($\mu g/m^3$)	7.57 (7.32, 7.88)	8.87 (7.23, 10.57)	10.36 (8.82, 12.00)
PPM_{10} ($\mu g/m^3$)	3.95 (3.82, 4.22)	7.61 (5.95, 9.70)	7.10 (5.79, 8.06)
$NPPM_{10}$ ($\mu g/m^3$)	10.27 (9.97, 10.73)	11.93 (7.68, 15.86)	17.32 (15.21, 19.46)
$NPPM_{2.5}$ ($\mu g/m^3$)	4.56 (4.34, 5.01)	12.04 (5.41, 18.76)	10.90 (8.74, 12.27)
NPcoarse ($\mu g/m^3$)	5.76 (5.61, 5.91)	5.70 (4.87, 6.63)	6.96 (6.12, 7.86)

on primary PM and BS, consistent with the earlier findings of Fuller and Green (2006 cited by Pirani et al. 2015). The large decrease in PNC was most likely due to a decrease in the sulphur content of diesel in 2008 which also contributed to decreased sulphate concentrations.

Comparing the predictive distribution of the deaths for 2012 vs 2005, a reduction in respiratory mortality was found, corresponding to an average percentage change in the posterior predictive distributions of −3.51% (95% CI: −0.12%, −5.74%). Based on the observed number of deaths for respiratory-related diseases which occurred in 2005, expect an average reduction in mortality of approximately 270 subjects.

Fig 14: Heatmap of posterior probability that day t belongs to one of the three representative clusters. (Pirani et al. 2015)

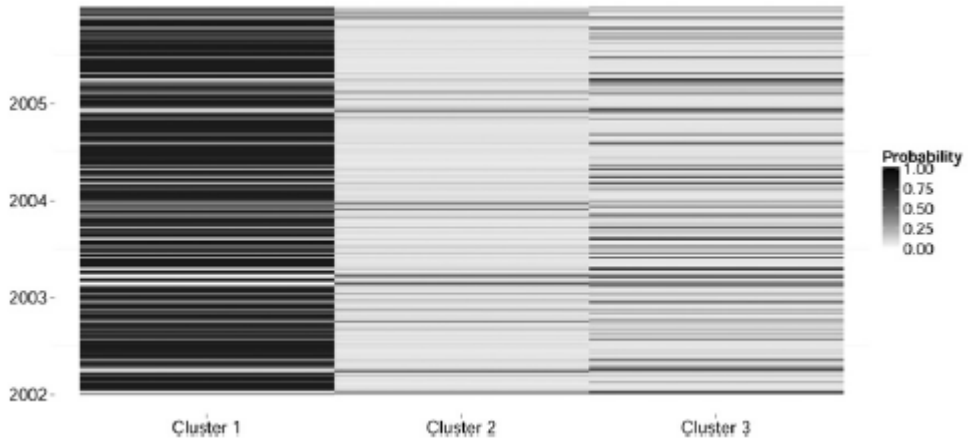

Fig 15: Posterior estimates (mean and 95% CI) for the coefficients of the natural cubic spline of time (left panel) and natural cubic spline of temperature (right panel). (Pirani et al. 2015)

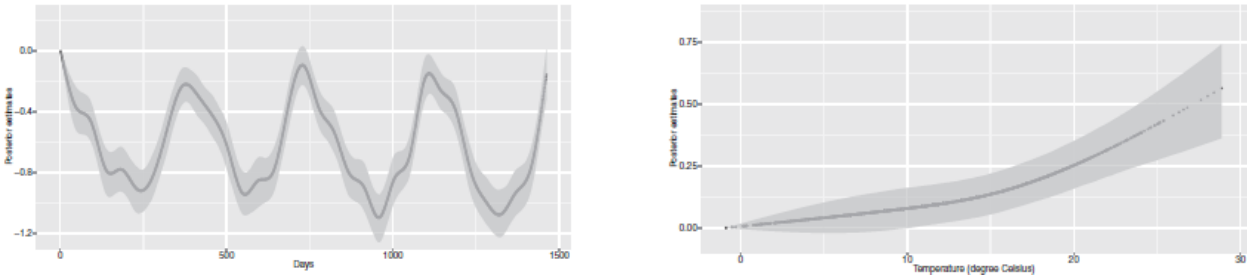

2.6- Saharan dust and mortality in Emilia-Romagna (Italy)

Fig 16: Saharan dust spreading to Emilia-Romagna as captured by the Moderate Resolution Imaging Spectroradiometer (MODIS) instrument on the NASA Aqua satellite. The boundaries of the Emilia-Romagna region and the location of the Monte Cimone station (CMN) are shown. (Sajani et al. 2011)

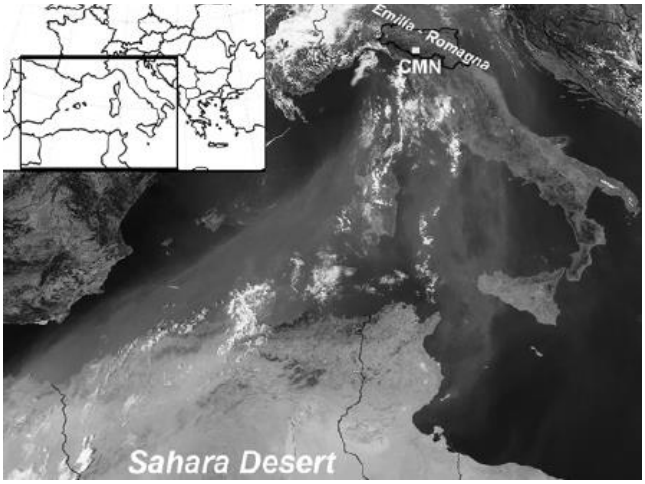

Desert dust is one of the greatest sources of natural aerosols in the atmosphere, representing about 37% of the total (natural and anthropogenic) emission of atmospheric primary aerosols (cited by Penner et al.2001).

Saharan events can also contribute to exceedances of the PM_{10} daily European Union limit (and WHO guideline value) of 50 mg/m³.

Saharan dust mobilisation has a great impact on the environment climate variability and, perhaps, human health.

A previous study focused on paediatric asthma accident and emergency admissions in the Caribbean island of Trinidad (cited by Sajani et al. 2011), showing an increase in respiratory health effects in association with Saharan dust days (SDD). An analysis of morbidity in Cyprus (Middleton et al. 2008 cited by Sajani et al. 2011) showed an increased risk of hospitalisation on Saharan dust storm days, particularly due to cardiovascular causes.

Table 11: Resume of principal information about the work by Sajani et al. 2011

Site	Aim	Period	Method
Barcellona Spain	investigate SDD effect modification on the particulate matter-mortality concentration response function, and assess the effects of SDD on natural, cardiovascular and respiratory mortality.	18 months	Case crossover design

This study aimed at assessing the effects of SDD on mortality in Emilia Romagna, a region in the Po basin of northern Italy (fig. 16). In this vast flat area surrounded by mountains and often experiencing high levels of air pollution, Saharan dust episodes have been regularly monitored since 2002 at the Italian National Research Council (CNR) 'O. Vittori' background station on Monte Cimone (CMN), the highest peak in the northern Apennine mountains (2165 m above sea level). This station belongs to the Global Atmosphere Watch programme of the World Meteorological Organisation.

2.6.1- METHODS

The specific objectives of the study were: (i) to investigate SDD effect modification on the particulate matter-mortality concentration – response function, and (ii) to assess the effects of SDD on natural, cardiovascular and respiratory mortality.

Exposure to particulate matter was expressed in term of particles with aerodynamic diameter <10 mm (PM_{10}). Population exposure to Saharan dust transport was expressed in terms of a dichotomous variable classifying the study

period in days affected (SDD) and not affected by Saharan dust transport (non-SDD).

2.6.2- statistical analysis

The epidemiological approach was based on a time-stratified Case - crossover design which is an adaptation of the common retrospective case control design. It was proposed by Maclure (cited by Sajani et al. 2011) to study the effects of transient, intermittent exposures on the subsequent risk of rare acute-onset events in close temporal proximity to exposure. This approach compares exposures during the period of time of death (case period) with one or more periods when death did not occur (control periods). Various sampling strategies were used to select control periods to estimate the effect of air pollution exposures on the health outcome of interest. Referent sampling schemes specific to air pollution epidemiology use reference periods both before and after the time of the event (bidirectional referent sampling) as a method to reduce bias due to temporal trends in exposure and outcome variables. In this study, control days were selected from the same day of the week, month and year as case days, following the time-stratified design which has been demonstrated to be the most appropriate for case e crossover studies of acute air pollution effects. The association of Saharan dust outbreaks and PM_{10} concentration with mortality was estimated using conditional logistic regression, adjusted for apparent temperature, holidays, summer population decrease (7-22 August), flu epidemic weeks and heat wave days. An apparent temperature confounding effect was considered following the approach already adopted within an Italian country-wide study on the health effects of PM_{10}. Heat wave days were defined as those days with mean apparent temperature above 308C for at least the 2 preceding days. This definition is very similar to that adopted in the Barcelona study and it corresponds to the definition of the alert level of the regional heat warning system. Influenza epidemics were defined on the basis of the weekly estimates of influenza incidence, as reported by the influenza surveillance system of the Italian National Institute of Health. Flu epidemics weeks were defined as the weeks with regional incidence higher than two new well-diagnosed flu cases/week/1000 patients.

Basically, two models were applied to analyse the data. First a model applied without insertion of the SDD variable. Then applied a model including, in addition to PM_{10} and SDD as principal variables, an interaction term between them to test

for effect modification induced by SDD on the PM_{10}-mortality concentration e response function. Finally, PM_{10} and SDD were inserted in a model as independent variables, that is, without
interaction.

Because of the higher risks associated with PM_{10} exposures during the hot season reported in several studies (Nawrot et al. 2007),(Peng et al. 2005) (cited by Sajani et al. 2011), separate estimates were undertaken for the period May e September (hot season) and October e April (cold season).

The statistical package R was used for the analyses.

2.6.3- RESULTS

Eighty-two Saharan events (ie, consecutive days affected by Saharan dust transport) were identified in the study period, accounting for 16% of the total days with available SDD classification. Classification of dust events was available for 77% of the total days, with missing classifications much more frequent during the cold season. The frequency of dust days according to the more restrictive definition of SDD was 11%. This definition will be used in the presentation of results unless otherwise specified. The dust events showed a marked seasonal pattern, with 72% of the dust events occurring between April and September.

The annual PM_{10} average concentration in the study area was 41 μg/m³, with approximately 25% of days exceeding the EU limit. A brief description of PM_{10} distributions for the different time periods (whole year, cold and hot seasons) as well as for SDD and non-SDD is reported in table 12. Similar average concentrations were found for PM_{10} during the SDDs and non-SDDs even though higher particulate concentrations for the SDDs were found for the hot season. The Wilcoxon ManneWhitney U test was applied to compare averages of PM_{10} concentrations on SDDs and non-SDDs. No significant differences were found for whole year and cold season averages. Significantly higher PM_{10} average concentrations on SDDs were found for hot season averages.

These results focus on the elderly because, as expected (Pope III et al. 2006) (cited by Sajani et al. 2011), they were found to be at greater risk in relation to both PM_{10} and SDD. In particular, unless otherwise stated, the results are presented for people aged 75 or older to allow comparison with the Barcelona study.

First a model was applied to assess the association between mortality and PM_{10} exposure without the insertion of the SDD variable. ORs were estimated for the same day (lag 0) to 4 days after exposure (lag 4). It found strongest effects at lag 1 and declining effects towards lag 4 (fig. 16).

Table 12 : Summary statistics for PM_{10} mass concentration distributions (mg/m³) for Saharan and non-Saharan dust days (Sajani et al. 2011)

					Percentiles				
	Num	Mean	SD	Min	25th	50th	75th	Max	IQ
Whole year									
Distribution of daily concentrations									
All days	1614	41	23	7	25	35	52	164	27
Saharan dust days	203	38	18	10	25	34	50	102	25
Non-Saharan dust days	1034	42	25	7	24	35	52	164	28
Distribution of differences in exposure between cases and controls									
	125100	−0.4	27.4	−127	−14	0	13	127	27
Hot season									
Distribution of daily concentrations									
All days	673	28	11	7	21	27	35	66	14
Saharan dust days	130	32	12	10	22	29	40	66	18
Non-Saharan dust days	467	27	9	7	20	26	33	55	13
Distribution of differences in exposure between cases and controls									
	47862	−0.6	13.4	−52	−9	−1	8	52	17
Cold season									
Distribution of daily concentrations									
All days	941	51	25	9	32	47	63	164	31
Saharan dust days	73	50	21	10	30	52	66	102	36
Non-Saharan dust days	567	54	27	9	34	50	67	164	33
Distribution of differences in exposure between cases and controls									
	77238	−0.2	33.2	−127	−20	0	20	127	40

The rise in natural mortality per 10 µg/m³ PM_{10} concentration increase (lag 1) was 0.4% (95% CI -0.2% to 1%) for the whole year model and 4.6% (95% CI 1.8% to 7.3%) for the hot season model. Also was tested lag 1 and obtained similar results. On the other hand, applying the same model only to the days when dust classification was available raised the risk per 10 µg/m³ PM_{10} concentration increase to 0.7% (95% CI _0.1% to 1.6%). It was not find heterogeneity among towns (p for heterogeneity with regard to natural mortality=0.67).

Table 13 shows the findings of models including, in addition to SDD and PM_{10} as principal variables, the interaction term between them. No evidence of effect modification of SDD on the PM_{10}-mortality relationship was found for any season or natural, cardiovascular or respiratory mortality (p value for interaction term>0.22).

Table 14 shows the results of the models with SDD and PM_{10} considered as independent variables. Various combinations was tested of lags for both PM_{10} and SDD (from lag 0 to lag 3). The strongest associations were found at lag 1 for both variables even though SDD was significantly associated with respiratory effects up to lag 3. The mean difference in exposures between cases and controls was -0.4 µg/m³ for the whole year, -0.6 µg/m³ for the hot season and -0.2 µg/m³ for the cold season. The average number of deaths per day was similar during the SDDs (21.6, 9.8 and 2.1 for natural, cardiovascular and respiratory deaths, respectively) and non-SDDs (22.0, 10.1 and 2.1, respectively).

An influence of dust outbreaks on mortality for all aggregated causes for both the whole year models and the hot season models was found. Dust effects were particularly evident for respiratory mortality, which increased by 22.0% (95% CI 4.0% to 43.1%) on the SDDs in the whole year model and by 33.9% (8.4% to 65.4%) in the hot season model. No additional risk was found during the cold season. The rise in natural mortality per 10 µg/m³ PM_{10} concentration increase was 0.8% (95% CI 0% to 1.6%) for the whole year model and 4% (95% CI 0.6% to 7.4%) for the hot season model.

Additional analyses were also carried out for other age groups. Models applied to people of all ages, those aged 65 or older and those aged 85 or older gave very similar results. Models applied to the <75-year-old age group confirmed a higher risk for respiratory mortality during dust days (table 14) even though the associations were not statistically significant and the confidence intervals were very large (OR 1.428 (95% CI 0.934 to 2.185) for the whole year model and 1.734 (95% CI 0.981 to 3.062) for the hot season model. Overall, no effect was found in this age group for cardiovascular and natural mortality.

Table 13: OR and 95% CIs for the association of daily exposure to Saharan dust and PM_{10} with natural, cardiovascular and respiratory mortality for people aged 75 or above (Sajani et al. 2011)

	SDD OR (95% CI)	PM_{10}* (no SDD) OR (95% CI)	PM_{10}* (SDD) OR (95% CI)	Interaction PM_{10}*—SDD p Value
Whole year				
Natural	1.080 (0.950 to 1.229)	1.008 (1.000 to 1.016)	1.000 (0.965 to 1.036)	0.55
Cardiovascular	1.092 (0.900 to 1.325)	1.003 (0.991 to 1.015)	0.992 (0.941 to 1.046)	0.61
Respiratory	1.320 (0.871 to 2.001)	1.016 (0.991 to 1.041)	0.998 (0.892 to 1.115)	0.69
Hot season				
Natural	1.169 (0.940 to 1.453)	1.048 (1.011 to 1.086)	1.016 (0.922 to 1.119)	0.31
Cardiovascular	1.285 (0.923 to 1.788)	1.046 (0.992 to 1.104)	0.987 (0.853 to 1.142)	0.22
Respiratory	0.964 (0.478 to 1.945)	1.064 (0.938 to 1.206)	1.171 (0.849 to 1.615)	0.34
Cold season				
Natural	0.949 (0.726 to 1.241)	1.005 (0.997 to 1.014)	1.015 (0.964 to 1.070)	0.31
Cardiovascular	0.895 (0.599 to 1.338)	1.000 (0.988 to 1.012)	1.020 (0.943 to 1.103)	0.22
Respiratory	0.777 (0.322 to 1.875)	1.008 (0.983 to 1.033)	1.046 (0.884 to 1.239)	0.34

Table 14 : OR and 95% CIs for the association of daily exposure to Saharan dust and PM_{10} with natural, cardiovascular and respiratory mortality (Sajani et al. 2011)

	≥75 Years old		<75 Years old	
	SDD OR (95% CI)	PM_{10}* OR (95% CI)	SDD OR (95% CI)	PM_{10}* OR (95% CI)
Whole year				
Natural	1.042 (0.992 to 1.095)	1.008 (1.000 to 1.016)	0.960 (0.882 to 1.044)	1.009 (0.995 to 1.022)
Cardiovascular	1.043 (0.969 to 1.122)	1.002 (0.991 to 1.014)	0.907 (0.763 to 1.079)	1.014 (0.988 to 1.040)
Respiratory	1.220 (1.040 to 1.431)	1.015 (0.991 to 1.040)	1.428 (0.934 to 2.185)	0.990 (0.926 to 1.059)
Hot season				
Natural	1.050 (0.986 to 1.119)	1.040 (1.006 to 1.074)	0.957 (0.860 to 1.065)	0.984 (0.932 to 1.038)
Cardiovascular	1.053 (0.957 to 1.158)	1.032 (0.983 to 1.083)	0.858 (0.685 to 1.075)	0.963 (0.864 to 1.073)
Respiratory	1.339 (1.084 to 1.654)	1.095 (0.979 to 1.223)	1.734 (0.981 to 3.062)	1.140 (0.845 to 1.538)
Cold season				
Natural	1.005 (0.925 to 1.092)	1.006 (0.997 to 1.014)	0.995 (0.860 to 1.151)	1.010 (0.996 to 1.024)
Cardiovascular	1.003 (0.888 to 1.133)	1.000 (0.988 to 1.013)	1.064 (0.799 to 1.417)	1.016 (0.989 to 1.044)
Respiratory	0.967 (0.740 to 1.265)	1.009 (0.984 to 1.034)	0.980 (0.489 to 1.963)	0.985 (0.920 to 1.055)

Results were qualitatively similar using the broader definition of SDDs, even though the increase in mortality associated with dust events was generally lower. Particularly, compared to the most restrictive SDD definition, the ORs associated with SDD with respect to natural mortality decreased from 1.042 to 1.001 for the whole year model and from 1.050 to 1.014 for hot season model.

2.7- $PM_{2.5}$ exposure and health impacts

Air pollution is one of the biggest environmental health risks. In Finland, fine particles ($PM_{2.5}$) were recently evaluated to be the most harmful ambient air pollutant Several health outcomes are related to $PM_{2.5}$ exposure. The associations are typically quantified as relative risks or hazard ratios in epidemiological studies. Traditionally, concentration response relationships for $PM_{2.5}$exposure have been assumed to be linear or log-linear. These mainly work for low-exposure levels but lead to unrealistically large impacts in areas where the concentrations are very high.

Table 15: Resume of principal information about the work by Korhonen et al. 2019

Site	Sampling Method	Aim	Period
Finland	The atmospheric chemical transport model SILAM	systematically quantify the impact of the spatial resolution on population-weighted mean concentration (PWC), its variance, and mortality attributable to fine particulate matter ($PM_{2.5}$) exposure	2015

Table 15 shows the principal information used for the methods of evaluating exposures to $PM_{2.5}$ and estimate the health effect.

Apply the method used by Punger and West (2013 cited by Korhonen et al. 2019) on two modelled air quality datasets for Finland in 2015. And then study the sensitivities of predicted population-weighted $PM_{2.5}$ concentrations, originated (i) from the national Finnish sources and dispersion and the long-range transport

modelled with SILAM, and (ii) from local Finnish sources modelled with FRES. The chemical and physical transformation of particulate matter and gaseous pollutants are included in the computations by the SILAM model, but these are not allowed for by the FRES model. Also investigate the influences of the spatial resolution on the associated predicted health impacts.

It was used predicted fine-resolution concentration datasets and spatial population distributions as input datasets in this analysis. Based on these fine-resolution datasets, It was produced aggregated datasets at coarser resolutions (1, 5, 10, 30, and 50 km), simply by spatially averaging the modelled concentrations. The results of this study therefore include the impacts of the spatial averaging of the dispersion simulations with 1-km grid cell size computed with a combination of high-resolution emission fields (250 m) and coarse resolution of meteorological data (15 km). Therefore, the results present the lower limits of the influence of model resolution. For actual model computations that would also use finer scale meteorological data, the influence of the coarser resolution on the population-weighted concentrations and the associated health impacts (in comparison with a finer resolution) would most likely be relatively larger

Fig 17: Total annual primary $PM_{2.5}$emissions (22 Gg) by sources in Finland in 2015 calculated with FRES model at 250-m resolution. (Korhonen et al. 2019)

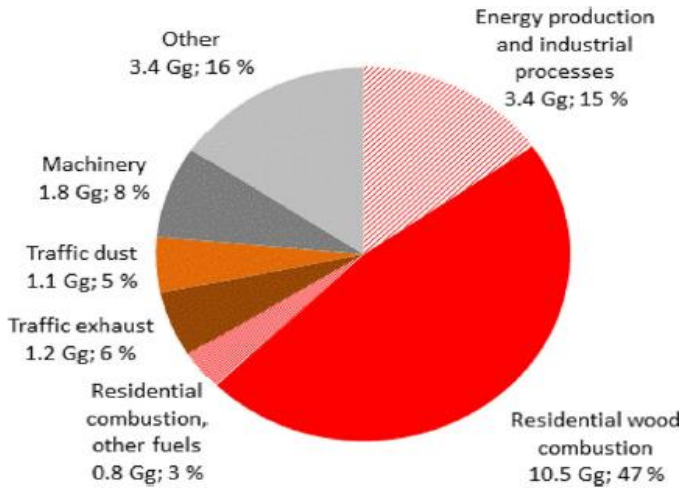

2.7.1- regional particle emissions and concentrations

The high-resolution modelling relied on the national $PM_{2.5}$ emission data, calculated at the Finnish Environment Institute (SYKE) with the FRES model

(Karvosenoja 2008 cited by Korhonen et al. 2019), at 250-m spatial resolution for area sources and an exhaustive list (n = 581) of point sources in Finland. The total annual primary $PM_{2.5}$ emissions in 2015 in Finland were 22 Gg (point sources 3.4 Gg; area sources 18.7 Gg) (Fig 17).

Two separate modelling systems were used to estimate the $PM_{2.5}$ concentrations and the impacts of the Finnish emission sources.
These were (i) the chemical transport model SILAM, which was used to estimate the $PM_{2.5}$ concentrations originated both from the local and the regional sources and (ii) the source-receptor matrices (SRMs) included in the FRES model to estimate the concentrations caused by local primary $PM_{2.5}$ sources. The computations using the SILAM model include also the secondary particulate matter, whereas the FRES computations include only the local primary particulate matter emissions up to 10 (traffic) and 20 km (residential combustion) distances.

The SILAM v5.5 dispersion model developed at the Finnish Meteorological Institute (FMI) (Sofiev et al. 2015 cited by Korhonen et al. 2019) was used to estimate the $PM_{2.5}$ concentrations, including also the LRT contributions. It is currently exploited on a daily basis in the national operational services, providing the air quality forecasts in global, European, and Fennoscandian domains. The set-up used for the SILAM model computations in this study contains four computational domains. The largest domain is global. The second largest domain is European, including the whole Europe, parts of the Northern Africa, and the western parts of Asia. The third domain includes Northern Europe, and the fourth domain includes the geographical area of Finland. Large-scale computations over the globe and Europe (1.44 degree and 0.5 degree, respectively) were required to generate physically realistic boundary conditions for the nested model runs for the Finnish domain. For the computations in the highest-resolution domain, the internal model time step was selected to be 1.5 min and 1 h for the model output. The spatial resolutions of the model output were 0.02° in longitudinal and 0.01° in latitudinal dimensions (these correspond to distances of the order of 1.1 km).

In vertical direction, the model considered 11 layers of different thickness from 20 m near the ground up to 2000 m outside of planetary boundary layer (Sofiev 2002; Sofiev et al. 2010 cited by Korhonen et al. 2019). The chemical transformations of atmospheric constituents were taken into account, and wet and dry depositions from the atmosphere to the underlying surfaces were calculated on every time step. The meteorological fields were extracted from the European Centre

of Medium-Range Weather Forecast (ECMWF) integrated forecast system (IFS). These data had the spatial resolution of about 15 km, with an update frequency of 3 h.

The primary fine particulate matter (P $PM_{2.5}$) concentrations originating from Finnish sources were estimated with the FRES model, using SRMs that were based on computations using a Gaussian dispersion model UDM-FMI. For computing the SRM's, meteorological data for ten different locations in Finland, for a period of 5 to 6 years (2000–2005) were used. The emissions and dispersion were taken into account on a resolution of 250 m× 250 m. Separate SRMs were created for emission sources with release heights of 2 m, dispersion extending to 20 km × 20 km area from each emission grid cell (vehicular traffic exhaust and dust and machinery), and 7.5 m release height extending to 40 km × 40 km area (residential combustion and other area sources, e.g., agriculture, peat production, small heating plants). The source-receptor matrices were evaluated separately on a monthly level, for ten spatial domains which correspond to the abovementioned locations in Finland. The computation of the previously used coarser SRMs at 1-km resolution has been presented in Karvosenoja et al. (2011 cited by Korhonen et al. 2019).

2.7.2- Population data and exposures

Population grid data at 1-km resolution presented in ETRS-TM35FIN coordinate reference system were obtained from Statistics Finland for December 31, 2015 (Statistics Finland 2017 cited by Korhonen et al. 2019). The number of total population is available for all inhabited cells (100,338). Population-weighted concentrations were calculated for (i) whole of Finland and divided into (ii) urban and (iii) rural areas, using 200 inhabitants per square kilometre as a threshold value between urban and rural areas. Population count at 1-km resolution was used to calculate PWC of $PM_{2.5}$ and local P $PM_{2.5}$ to all areas at 1- to 50-km resolution. Population data at 1-km resolution was also used to calculate PWC of primary $PM_{2.5}$ for five emission sectors divided to urban and rural areas at resolutions ranging from 250 to 50 km. In addition, Building and Dwelling Register 2014 (BDR) population data was used to calculate PWC of overall local and source-specific P $PM_{2.5}$ to whole of Finland at 250-m resolution to get more accurate estimate of exposure. PWCs in Finland in 2015 for $PM_{2.5}$ were estimated with Eq. (9).

$$\text{PWC} = \frac{\sum_{i=1}^{N} C_{m,i} P_i}{\sum_{i=1}^{N} P_i} \quad \textbf{(9)}$$

where N is the number of population in each grid cell, $C_{m,i}$ is the modelled concentration in i^{th}cell and P_i is the population in ith cell.

2.7.3- Comparison of health impacts

Deaths attributable to $PM_{2.5}$ exposure in the whole of Finland were evaluated using PWCs from SILAM and FRES models. For both models, the PWCs were evaluated on the following resolutions: 1 km, 5 km, 10 km, 30 km, and 50 km. For the FRES results, 250-m resolution was used as well. Attributable deaths were estimated using log-linear concentration-response function (relative risk (RR): 1.062) from Heroux et al. (2015 cited by Korhonen et al. 2019). In addition, Used supra-linear integrated exposure response functions (IER) for ischemic heart disease, stroke, chronic obstructive pulmonary disease, and acute lower respiratory infections (children) for SILAM estimates. Due to the non-linearities in the IER functions, was take into account the exposure distribution by assuming a normal distribution. Deaths calculated with IER functions were summed up and the total attributable deaths were presented. Deaths attributable to $PM_{2.5}$ are calculated using attributable incidence (AI) approach shown in Eq. (10).

$$AI = PAF \times I = \frac{f \cdot (RR_E - 1)}{f \cdot (RR_E - 1) + 1} \times I \quad \textbf{(10)}$$

where AI is deaths attributable to $PM_{2.5}$ exposure, PAF is the population attributable fraction, I is the background incidence rate (in this case, mortality), and f is the fraction of the target population exposed to $PM_{2.5}$ (100%), RR_E is the relative risk of the population at the prevailing exposure level, calculated as RR_E = exp.(E × ln (RR_1)) in which RR1 is the relative risk estimate per unit of exposure and E is the mean population exposure.

2.7.4- Population-weighted concentrations

Annual population-weighted concentration (PWC) of $PM_{2.5}$calculated with the SILAM model was 5.1 μg/m³ at 1-km resolution.

Population weighted primary fine particulate concentration originated from local emission sources, calculated with the FRES model concentrations at 250-m resolution was 1.6 μg/ m³. Difference to the corresponding results computed on 1-km resolution was modest, but decrease of estimated concentration was substantially larger for the results computed on coarser resolutions. Exposure estimate calculated with 50-km resolution was 70% lower than estimation done with 250-m resolution. Maximum concentration of P $PM_{2.5}$in populated grid cells decreased with coarser resolution and was about 80% lower at 50 km resolution compared with 1 km.

Residential combustion had the highest contribution to the overall concentration of primary $PM_{2.5}$ at all resolutions. With the exception of P $PM_{2.5}$ concentrations originating from machinery and other traffic sources (ca. 15%decrease), there was no great difference in exposures between 250-m and 1-km resolutions. Population-weighted concentration originated from traffic dust was least affected to resolution change between 1- and 5-km resolution and PWC of residential combustion at resolutions coarser than 5 km. Population-weighted primary $PM_{2.5}$ concentration of residential combustion calculated at 50-km resolution was about 40% of those estimated with 250-m resolution. PWCs originated from traffic sources at 50-km resolution were only ca.15–20% of those calculated at original 250-m resolution. Decrease of maximum concentrations in populated grid squares was also greater from traffic sources compared with residential combustion and other sources.

When resolution was changed to be coarser, the exposure distribution shifted towards lower concentrations (Fig. 18). Number of people (ca. 1.3 million) exposed to $PM_{2.5}$ concentrations that were, e.g., over 6.0 μg/m3 calculated at 1-km resolution was considerably higher, when compared with the corresponding results computed using averaged 50- km resolution (ca. 100 k). Averaging the local primary fine particle exposures to coarser resolution had much greater influence to exposure distribution compared with the results for particulate matter ($PM_{2.5}$) exposure distribution. At 50-km resolution, almost whole population was exposed to P $PM_{2.5}$ levels under 1 μg/m³, whereas at the resolution of 1 km, the highest exposures were over 4 μg/m³ and at 5-km resolution over 3 μg/m³.

Fig 18: Exposure distributions of a $PM_{2.5}$ and b local primary $PM_{2.5}$ in 2015, modelled with SILAM and FRES at 1-km and 250-m resolution, respectively and averaged to coarser resolutions of 1 km, 5 km, and 50 km. (Korhonen et al. 2019)

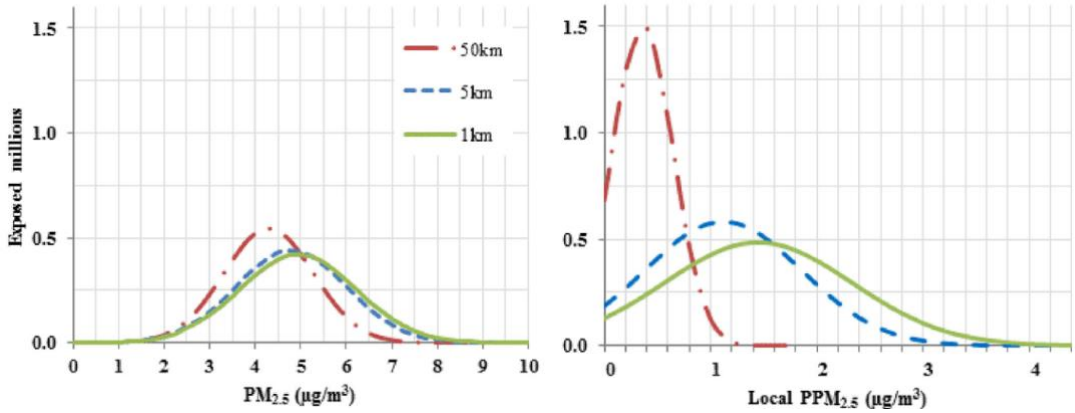

(a) SILAM (b) FRES

2.7.5- Results

Sensitivities of PWCs of $PM_{2.5}$ and primary $PM_{2.5}$ and attributable mortality to resolution change were studied. Concentrations modelled with SILAM at 0.02° longitudinal × 0.01° latitudinal resolution and FRES with 250 m resolution were averaged to coarser resolutions (1–50 km).

2.8- Study on particulate matter, and human health risk based of PM_{10} (Volos)

Air pollution has been a prominent feature in large cities and urban areas for at least two centuries now, mainly due to industrialization. Nowadays, air pollution is characterized by a number of primary (sulphur oxides, nitrogen oxides, CO, volatile organic compounds) and secondary pollutants (ozone, non-sea-salt sulphate, and secondary organic aerosols) which contribute each to the observed atmospheric quality.

Table 16: Resume of principal information about the work by Emmanouil et al. 2017

Site	Sampling Method	Aim	Period
Volos	Samples were collected for 24 h on conditioned and pre-weighed by means of low-volume samplers at a rate of 2.3 m3 h¯ 1, Loaded filters were conditioned again before weighing. A microbalance with a resolution of 0.01 mg was used. Filter samples were stored in a cool and dark place until analysis.	Assess the PM pollution profile in Volos for the last half decade and, based on a small current campaign, to investigate possible correlations between sources and observed levels.	5-year between 2009 and 2014.

Table 16 shows the Resume of the principal information about a PM_{10} sampling, and metals and other elements in the PM_{10} mass in Volos City.

Fig 19: Map of sampling area (Volos, Greece); black spot is the sampling station area. (Emmanouil et al. 2017)

The City of Volos is the capital of Magnesia Prefecture in the administrative region of Thessaly, Greece (Fig 19). Volos is the third largest commercial port of mainland Greece towards the Aegean Sea, with two industrial parks in its outskirts as well as one of the largest cement factories in Northern Greece. The current population (2011) of the city of Volos is 144,449 inhabitants (Hellenic Statistical Authority 2015 cited by Emmanouil et al. 2017). The presence of circumferential mountainous terrain creates local air turbulences making air exchange problematic. Similar circumstances (concomitant port, industrial, and commercial activities, traffic congestion, mountain obstruction) prevail also in other middle-sized Greek cities (Pikridas et al. 2013 cited by Emmanouil et al. 2017).

2.8.1- Ambient PM_{10} sampling and Elemental analysis in collected PM particles

PM_{10} sampling was carried out during 22 May 2014–11 June 2014 at the University of Thessaly, Department of Planning and Regional Development, in the city center.

Samples were collected for 24 h on conditioned (48 h at 20 $\pm$1 ºC and 50 $\pm$ 5% relative humidity) and pre-weighed PTFE Whatman filters (Ø 47 mm, 1 µm pore size) by means of low-volume samplers (Leckel SEQ 47/50 Sequential Gravimetric Sampler, Enviro Technology Services PLC, London, UK) at a rate of 2.3 m^3h^{-1}, in accordance with the sampling procedure standardized in EN 12341 (1998 cited by Emmanouil et al. 2017) Loaded filters were conditioned again before weighing. A microbalance (Sartorius, Göttingen, Germany) with a resolution of 0.01 mg was used. Filter samples were stored in a cool and dark place until analysis.

The collected samples' filters were cut into halves. One half was used for the determination of V, As, Co, Cr, Cd and Sb by means of an electrothermal atomic absorption spectroscope (ET-AAS), the other half was analyzed by X-ray fluorescence (XRF) for Na, Mg, Al, Si, S, Cl, K, Ca, Ti, Cr, Mn, Fe, Ni, Cu, Zn, Ga, Ge, Br, Sn, Cs, Ba, Pt, Hg, Sr, and Rb.

2.8.1.1- ET-AAS and XRF

Wresting of total metal content was experienced through microwave digestion of the half filters with 2 mL concentrated HNO3 (65%, suprapure, Merck, Darmstadt, Germany) and 1 mL HF (40%, suprapure, Merck). All digestions were performed in a microwave oven (M625EG, Miele, Gütersloh, Germany). The oven is programmable, with a time resolution of 5 s, and has a maximum power of 1000 W. The following program settings were followed: 4 min at 300 W, 2 min at 450 W, and 2 min at 600 W. Pd (suprapure, Merck) was used as matrix modifier for Pb, Cd, As, and Sb, and Mg (suprapure, Merck) for V.

The digests were diluted to 10 mL by adding Milli-Q ultrapure water and analyzed by ET-AAS. Hollow single-element cathode lamps were used as radiation sources for all elements. The ET-AAS instrument was calibrated according to Karanasiou, Siskos, and Eleftheriadis (2005 cited by Emmanouil et al. 2017). Standards for calibration were obtained from Merck and Carlo Erba (Milano, Italy) and solutions were prepared by use of a Millipore Milli-Q System.

The analysis by XRF was performed on one half of the filter samples, without any processing. The secondary target-XRF spectrometer consisted of a side window low-power X-ray tube with a W anode (spot size 1.8–2.1 cm, max voltage 100 kV, current 6 mA, maximum power consumption 600 W). The characteristic X-rays emitted from the sample were detected by a Ge X-ray detector (PAN-32).

2.8.2- Calculation of contribution of sea salt and soil dust, and impact of desert dust to PM_{10}

The contribution of sea salt (μg m^{-3}) to PM_{10} was calculated through stoichiometry, assuming that Cl originates solely from sea salt. Non-sea salt sodium (nss Na) was calculated based on the crustal ratio Na/Al and total sea salt mass was calculated as the sum of Cl, ss Na and fractions of the concentrations of Mg and K (ss Mg and ss K), based at a standard sea water concentration of these species with respect to Na.

The contribution of soil dust (μg m^{-3}) was calculated on the basis of the sum of Al, Si, Ca, Ti and Fe plus the non-sea salt proportions (nss) of Na, Mg and K according to Karanasiou, Siskos, and Eleftheriadis (2009 cited by Emmanouil et al. 2017) and Amato et al. (2016 cited by Amato et al. 2015), with Ca being multiplied by a factor of 1.95 to account for CaO and $CaCO_3$as most abundant forms:

$$\text{Minerals} = [nss\ \text{Na}\ ] \times 1{,}35 + [nss\ Mg] \times 1{,}66 + [AI] \times 1{,}89 \times [Si] \times 2{,}14 + [nss\ k] \times 1{,}2 + [Ca] \times 1{,}95 + [Ti] \times 1{,}67 + [Fe] \times 1{,}43\ . \quad \textbf{(11)}$$

The impact of desert dust transport to the measured PM_{10} was examined based on calculated ratios of Ca/Fe, Ti/Fe and Mn/Fe which have been shown to demonstrate typical values during long-range dust transport events. When the actual data were similar to the published values, air mass backward trajectories were calculated for verification, for 160 h, using the hybrid single-particle Lagrangian integrated trajectory model (HYSPLIT) (Air Resources Laboratory 2015, cited by Emmanouil et al. 2017) for arrival heights of 300, 700 and 1000 m a.m.s.l. at 8.00 and 18.00 h UTC each day.

2.8.3- Human risk

Non-carcinogenic risk assessment for elements bound on PM_{10} was calculated via the hazard quotient (HQ) approach, which compares the actual exposure of humans (Cexp, μg m^{-3}) to a predefined reference toxicity value. The sum of HQs for each element is giving the cumulative hazard index (HI) which, when less than 1, shows that the risk is acceptable (Li et al. 2013 cited by Li et al. 2012). Exposure concentration has been calculated when an oral reference dose is available via the formula (Li et al. 2013 cited by Emmanouil et al. 2017):

$$C_{exp} = CA \times IR \times ET \times EF \times ED \; / \; BW \times AT \quad , \qquad \textbf{(12)}$$

or when an inhalation reference dose is available via the formula (Industrial Economics Incorporated 2009 cited by Emmanouil et al. 2017):

$$C_{exp} = (CA \times ET \times EF \times ED) \; / \; AT, \qquad \textbf{(13)}$$

where CA is the concentration of the metal in the air (μg m^{-3}), IR is the inhalation rate ($m^3 d^{-1}$), ET is the exposure time (h d^{-1}), EF is the exposure frequency (d a^{-1}), ED is the exposure duration (a), BW is the body weight (kg), and AT is the averaging time (h).

The 'local residents' (Industrial Economics Incorporated 2009 cited by Sandiford et al. 2009) parameters have been chosen as a worst case scenario and as such exposure is considered to be continuous with

IR = 0.55 $m^3 h^{-1}$,
BW = 70 kg.

Reference concentration values (RfCs) were extracted following a step-wise approach (Industrial Economics Incorporated 2009 cited by Emmanouil et al. 2017)

with endpoints preferentially chosen from the USEPA IRIS database (USEPA 2016 cited by Emmanouil et al. 2017).

2.8.4- Results

2.8.4.1- PM_{10} levels

Average annual PM_{10} values for the years 2009–2014 are shown in Fig 13. There is no exceedance of the 40 μg m^{-3} average annual limit set by Directive 2008/50/EC(cited by Emmanouil et al. 2017).

The mean seasonal PM_{10} concentrations for the period 2009 2014 are shown in Fig 21. The cold months January, February, November and December are characterized by higher PM_{10} concentrations than all the other months.

Days when exceedance of the EU set limit of 50 μg m^{-3} was noted are shown in Fig 22 (A). The percentage of days with concentrations above the EU daily limit value exceeded the maximum allowed value of 9.6% (35 out of 365 days) for almost all years (Fig 22 (B)). No repeating pattern was observed for each day within the week (data not shown).

2.8.4.2- Elemental concentrations

The most abundant elements measured were Na, S, Ca, Si, Fe, Al, K, Mg, Cl and Zn. Those of toxicological concern, i.e. As, Ni, Cd, Hg and Pb, were noted at lower concentrations than the former, abundant elements (mean values of 1.9, 3.0, 1.3, 0.1 and 37 μg m^{-3}, respectively).

Fig 20: Annual average PM_{10} concentrations during 2009–2014. (Emmanouil et al. 2017)

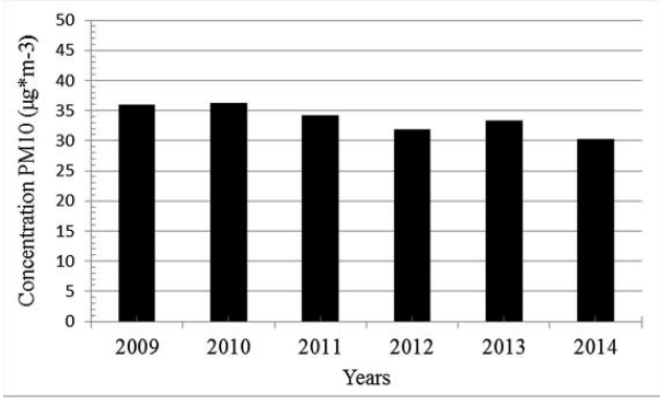

PCA correlations were explored for the elements of inhalation toxicological concern, namely As, Cd, Cr, Co, Mn, Ni, Pb, and V (Fig16). Hg and Sb were not included due to low number of valid samples. Three factors comprised 82% of total variance: Pb, Cd, Mn and Cr are grouped as first component (38.1%), V, Ni and As as second component (28.5%), Co as third component (15.6%).

Fig 21: Mean seasonal PM_{10}concentrations for the period 2009–2014. (Emmanouil et al. 2017)

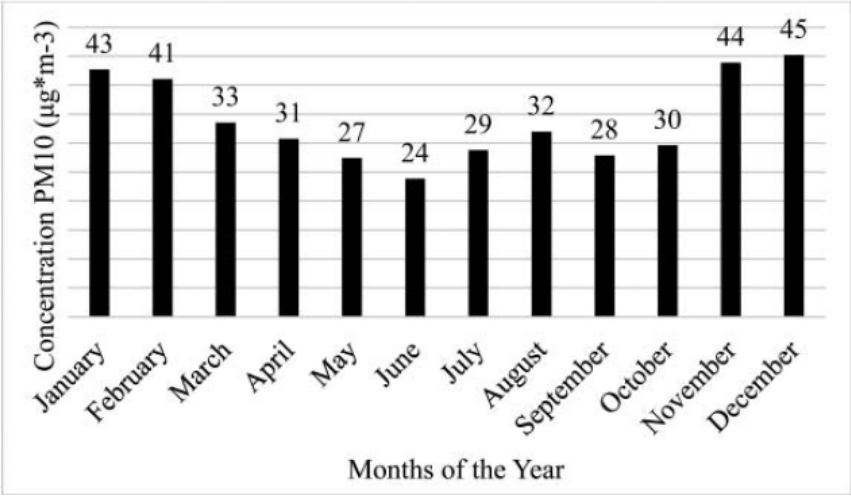

Fig 22: (A) Numbers of days at which mean daily PM_{10} concentrations exceeded the EU limit value relative to the numbers of days at which PM_{10} measurements were taken, from 2009 to 2014; (B) percentages of days at which the mean daily PM_{10} concentrations exceeded the EU limit. (Emmanouil et al. 2017)

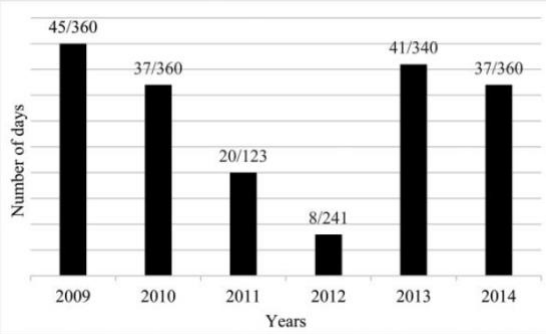

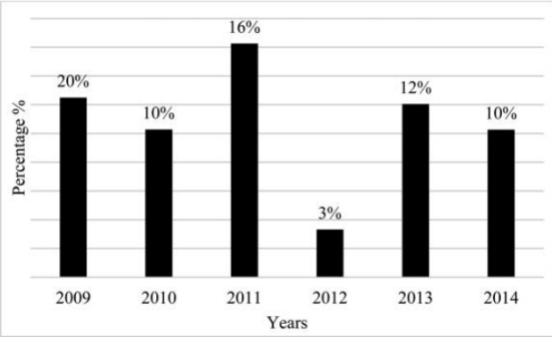

(A) (B)

Non-carcinogenic risk of elements can effectively be assessed as the HI, the sum of all HQs of each element. Monte Carlo simulation has been performed for the HQ of each element of toxicological concern and the HI resulting from all the eight elements considered for the samples collected during 22 May 2014–11 June 2014. HQ values greater than 1 indicated an unacceptable risk for V and Co. HI for all eight elements was also greater than 1.

Comparison of the ratios of Ca/Fe, Ti/Fe and Mn/Fe calculated during the present measurement campaign with those published by Eleftheriadis et al. (1999 cited by Emmanouil et al. 2017) as indicative of Sahara aerosol revealed seven days with similar ratios. For these dates, the HYSPLIT model was run; only on the 28th of May 2014 at 18:00 UTC, air masses passed over Sahara and ultimately reached Volos at arrival heights of 300 m a.m.s.l. (Fig 24). Thus, contribution of desert dust to measured PM10 through long-range transport was possible.

Fig 23: Three-dimension plot of PCA for eight elements of toxicological concern. (Emmanouil et al. 2017)

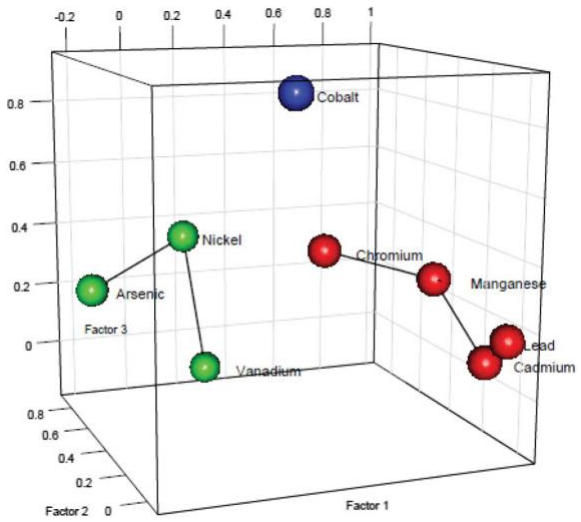

Regarding the other natural sources that may affect PM_{10} levels, i.e. sea salt and soil dust (Fig 25), the latter contributes on average 8.4% to the total PM_{10} mass, the former 12.4%.

Fig 24: Backward trajectories on 28 May 2014 at 08.00 and 18.00 UTC when long-range dust transport was possible. (Emmanouil et al. 2017)

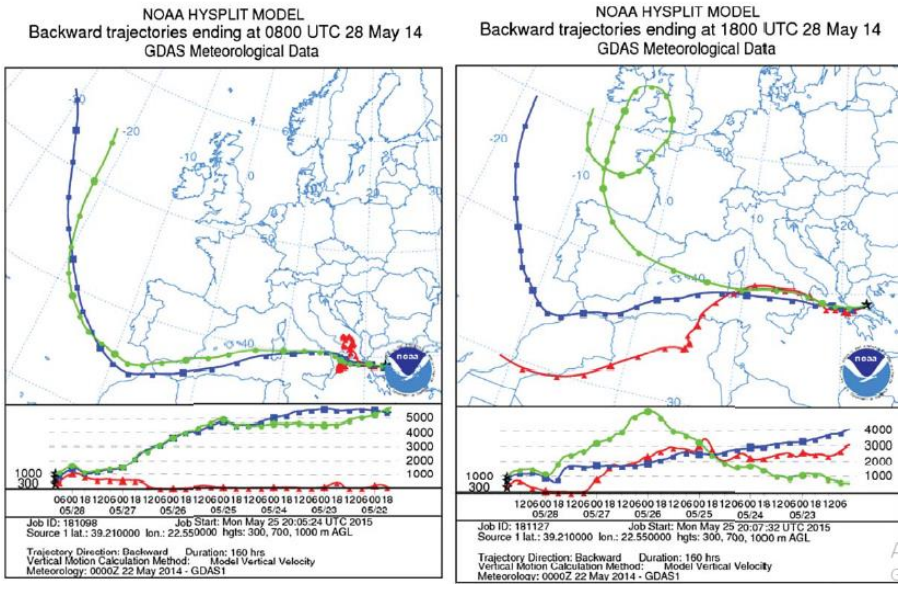

Fig 25: The % contribution of sea salt and soil dust in the mass of PM_{10} during the sampling period. (Emmanouil et al. 2017)

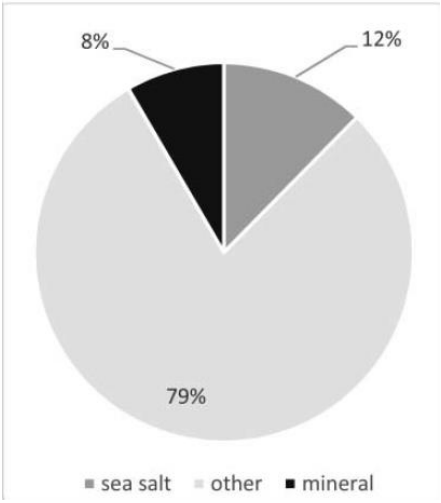

3-Conclusions

After reading about twenty articles related to the topic on the effect of pollutants on health, I analyzed a dozen of them concerning PM_{10}, $PM_{2.5}$ and NO_x specifically NO_2. The articles analyzed refer to studies in the urban area of some European countries, specifically Greece, Spain, Italy, Finland and the United Kingdom.

In these studies, various methodologies have been used to evaluate the effect of pollutants on the health of the population exposed to these types of pollutants.

NO_x has a negative effect on both health and the environment. The attributable risk (AR) represents the percentage increase in daily mortality for every 10 μg/m³ increase in the pollutant studied. The population AR is calculated based on the risk assessment methodology.

To better quantify the average health impact of PM on health, the Dirichlet process mixture models enables the better understanding of hidden structures in multipollutant health effects within time series analysis. This approach allows the identification of exposure metrics associated with respiratory mortality and provides a tool to assess the changes in health effects from various policies to control the ambient particle matter mixtures.

Finally, air pollution remains a global environmental threat and a public health risk.

Acknowledgment

Tanks to merciful Allah for all the countless gifts you have offered me, and thanks to my family for their love and support.

It is a great pleasure to acknowledge my deepest thanks and gratitude to **prof. Giorgo Passerini**, *professor of Technical Physics, Faculty of Engineering Polytechnic University,* for suggesting the topic of this essay, and his kind supervision. It is a great honour to work under his supervision.

I would like to express my deepest thanks and sincere appreciation to **Dr. Enrico Mancinelli,** for his encouragement, creative and comprehensive advice until this work came to existence.

I wish to acknowledge the support and great love of my family, my father **Ali**, my mother **Salma**, my brothers **Ayad**, **Loukman**, **Fouad**, **Zein Alabidin**, **Azmi** and **Charif**, my niece **Alissar**. They kept me going on and this work would not have been possible without their input. I am forever indebted to my parents for giving me the opportunities and experiences that have made me who I am.

I also thank my best friend **Martina Mattucci** for always being there for me as a sister.

References

Casquero-Vera, J. A., Lyamani, H., Titos, G., Borrás, E., Olmo, F. J., & Alados-Arboledas, L. (2019). Impact of primary NO2 emissions at different urban sites exceeding the European NO2 standard limit. *Science of The Total Environment*, *646*, 1117-1125.

Cilluffo, G., Ferrante, G., Fasola, S., Montalbano, L., Malizia, V., Piscini, A., ... & Ranzi, A. (2018). Associations of greenness, greyness and air pollution exposure with children's health: a cross-sectional study in Southern Italy. *Environmental Health*, *17*(1), 1-12.

Rivas, E., Santiago, J. L., Lechón, Y., Martín, F., Ariño, A., Pons, J. J., & Santamaría, J. M. (2019). CFD modelling of air quality in Pamplona City (Spain): Assessment, stations spatial representativeness and health impacts valuation. *Science of the Total Environment*, *649*, 1362-1380.

Linares, C., Falcón, I., Ortiz, C., & Díaz, J. (2018). An approach estimating the short-term effect of NO2 on daily mortality in Spanish cities. *Environment international*, *116*, 18-28.

Sajani, S. Z., Miglio, R., Bonasoni, P., Cristofanelli, P., Marinoni, A., Sartini, C., ... & Lauriola, P. (2011). Saharan dust and daily mortality in Emilia-Romagna (Italy). *Occupational and Environmental Medicine*, *68*(6), 446-451.

Samoli, E., Stergiopoulou, A., Santana, P., Rodopoulou, S., Mitsakou, C., Dimitroulopoulou, C., ... & Corman, D. (2019). Spatial variability in air pollution exposure in relation to socioeconomic indicators in nine European metropolitan areas: A study on environmental inequality. *Environmental Pollution*, *249*, 345-353.

Pirani, M., Best, N., Blangiardo, M., Liverani, S., Atkinson, R. W., & Fuller, G. W. (2015). Analysing the health effects of simultaneous exposure to physical and chemical properties of airborne particles. *Environment international*, *79*, 56-64.

Korhonen, A., Lehtomäki, H., Rumrich, I., Karvosenoja, N., Paunu, V. V., Kupiainen, K., ... & Karppinen, A. (2019). Influence of spatial resolution on population PM 2.5 exposure and health impacts. *Air Quality, Atmosphere & Health*, *12*(6), 705-718.

Emmanouil, C., Drositi, E., Vasilatou, V., Diapouli, E., Krikonis, K., Eleftheriadis, K., & Kungolos, A. (2017). Study on particulate matter air pollution, source origin, and human health risk based of PM10 metal content in Volos City, Greece. *Toxicological & Environmental Chemistry*, *99*(4), 691-709.

Ielpo, P., Mangia, C., Marra, G. P., Comite, V., Rizza, U., Uricchio, V. F., & Fermo, P. (2019). Outdoor spatial distribution and indoor levels of NO2 and SO2 in a high environmental risk site of the South Italy. *Science of the total environment*, *648*, 787-797.

Lian, G. D., Yuan, J., Brown, L. M., Kim, G. H., & Ritchie, D. A. (1998). Modification of InAs quantum dot structure by the growth of the capping layer. *Applied physics letters*, *73*(1), 49-51.

Volkamer, R., Jimenez, J. L., San Martini, F., Dzepina, K., Zhang, Q., Salcedo, D., ... & Molina, M. J. (2006). Secondary organic aerosol formation from anthropogenic air pollution: Rapid and higher than expected. *Geophysical Research Letters*, *33*(17).

Neophytou, A. M., Yiallouros, P., Coull, B. A., Kleanthous, S., Pavlou, P., Pashiardis, S., ... & Laden, F. (2013). Particulate matter concentrations during desert dust outbreaks and daily mortality in Nicosia, Cyprus. *Journal of Exposure Science & Environmental Epidemiology*, *23*(3), 275-280.